Heteroleptic Ter–Bidentate Cr(III) Complexes as Tunable Optical Sensitizers

Doistau, Benjamin; Collet, Guillaume; Acuna Bolomey, Emilio; Sadat-Noorbakhsh, Vida; Besnard, Céline; Piguet, Claude

How to cite

DOISTAU, Benjamin et al. Heteroleptic Ter–Bidentate Cr(III) Complexes as Tunable Optical Sensitizers. In: Inorganic Chemistry, 2018, vol. 57, n° 22, p. 14362–14373. doi: 10.1021/acs.inorgchem.8b02530

This publication URL: https://archive-ouverte.unige.ch/unige:111465
Publication DOI: 10.1021/acs.inorgchem.8b02530

Publication: *Inorg. Chem.* **2018**, *57*, 14362-14373. DOI:10.1021/acs.inorgchem.8b02530
Full data: https://www.unige.ch/sciences/chiam/piguet/

Heteroleptic Ter-bidentate Cr(III) Complexes as Tunable Optical Sensitizers

Benjamin Doistau,[a] Guillaume Collet,[a,†] Emilio Acuña Bolomey,[a] Vida Sadat-Noorbakhsh,[a] Céline Besnard,[b] and Claude Piguet*[a]*

[a] Department of Inorganic and Analytical Chemistry, University of Geneva, 30 quai Ernest Ansermet, CH-1211 Geneva 4, Switzerland

[b] Laboratory of Crystallography, University of Geneva, 24 quai Ernest Ansermet, CH-1211 Geneva 4, Switzerland

KEYWORDS

Chromium(III), complex, heteroleptic, lifetime, sensitizer, symmetry.

ABSTRACT

In order to exploit Cr(III) coordination complexes as sensitizers in supramolecular energy-converting devices, the latter optical relays should display long-lived excited states, broad emission bands and tunable spatial and electronic connections to activator units. An ad-hoc versatile strategy has been therefore developed for the preparation of a family of luminescent pseudo-octahedral $[CrN_6]$ chromophores made up of ter-bidentate heteroleptic $[Cr(phen)_2(N\text{-}N')]^{3+}$ complexes, where phen is 1,10-phenanthroline and N-N' stands for α,α'-diimine ligands possessing peripheral substituents compatible with both electronic tuning and structure extensions. As long as the ligand field in these $[CrN_6]$ chromophores remains sufficiently strong to avoid back intersystem crossing, photophysical studies indicate that the lifetime of the near-infrared emissive $Cr(^2E)$ excited state is poorly sensitive to

ligand-based electronic effects. On the contrary, a drop in symmetry, the coupling with high frequency oscillators and the implementation of sterical constraints in heteroleptic $[Cr(phen)_2(N\text{-}N')]^{3+}$ complexes affect both $Cr(^2E \rightarrow {}^4A_2)$ energies and $Cr(^2E)$ lifetimes. Altogether, $[Cr(phen)_2(phenAlkyn)]^{3+}$ (phenAlkyn = 5-ethynyl-1,10-phenanthroline) and $[Cr(phen)_2(dpma)]^{3+}$ (dpma = di(pyrid-2-yl)(methyl)amine) complexes mirror the favorable photophysical properties of homoleptic $[Cr(phen)_3]^{3+}$ and thus emerge as the best heteroleptic candidates for acting as sensitizers at room temperature, and below 100 K, respectively, in more complicated architectures.

INTRODUCTION

Cr(III)-containing coordination complexes have recently attracted a renewal of interest for their magnetic, redox and optical properties, which proved to be useful for various modern applications where this earth-abundant metal could advantageously replace rare ruthenium or platinum ores.[BD1,BD2] Firstly, the orbital-free magnetic moments of trivalent chromium complexes are ideally suited for rationalizing and optimizing (i) magnetic coupling,[BD3,BD4,BD5,BD6] (ii) zero-field splitting[BD7,BD8,BD9,BD10,BD11] and (iii) single-molecular magnet behavior[BD12,BD13] implemented in polymetallic architectures.[BD14,BD15,BD16,BD17] Secondly, the Cr(III) polypyridyl complexes are famous for displaying three successive ligand-centered[BD11] or one metal centered reductions,[BD36] which allows their incorporation into memory devices.[BD18] Thirdly, the strongly oxidative $Cr(^2E)$ spin-flip excited state can be exploited (i) in photo-cathodic solar cells (by grafting chromium polypydidyl complexes onto semi-conductor surfaces),[BD19] (ii) for carbon-carbon bond formation[BD20,BD21,BD22] and (iii) for water splitting and O_2 production.[BD23] Finally, the remarkable metal-centered optical properties of Cr(III) complexes associated with octahedral $[CrO_6]$ units found in solid oxides (weak ligand fields Δ and large Racah parameters B and C),[BD24,BD25,BD26,BD27,BD28] which gave rise to the first ruby lasers, can be completely reversed in coordination complexes with the preparation of $[CrN_6]$ chromophores (strong

ligand fields Δ and weak Racah parameters B and C)[BD29,BD30,BD31] programmed for acting as sensitizers in molecular lanthanide-based energy transfer upconversion.[BD32,BD33,BD34,BD35] The associated micro to millisecond lifetimes (τ_S) observed for the metal-centered excited-state levels in [CrN_6] complexes maximize energy transfer efficiency $\eta_{ET}^{S\rightarrow A}$ in sensitizer→activator pair (eq. 1)[BD39,BD40] and are therefore well-adapted for being harnessed for the sensitization of nearby activators in polymetallic assemblies ($k_S^{rad}\tau_S = \Phi_S$ corresponds to the intrinsic quantum yield of the donor, κ is the orientation factor between sensitizer and activator dipoles, n_r is the refractive index of the medium, N_{Av} is the Avogadro number in mol^{-1},[BD40] r is the separation between donor and acceptor and $J(\lambda)$ is the overlap integral between the emission spectrum of donor (S) and the absorption spectrum of the acceptor (A)).[BD41,BD42,BD43,BD44,BD45,BD46,BD47]

$$\eta_{ET}^{S\rightarrow A} = \frac{k_{ET}^{S\rightarrow A}}{k_{ET}^{S\rightarrow A} + k_S} = \left(1 + \frac{128\pi^5 n_r^4 N_{Av} r^6}{9(\ln 10)\kappa^2 J(\lambda) k_S^{rad}\tau_S}\right)^{-1} \quad (1)$$

Reasonably assuming comparable radiative rate constant (k_S^{rad}) for [CrN_6] complexes with similar symmetries, the Cr(^{2}E) excited state lifetime τ_S thus appears as the most relevant tunable parameter with $J(\lambda)$ and r for optimizing energy transfer efficiency ($\eta_{ET}^{S\rightarrow A}$). Despite these remarkable photophysical properties, alternative Ru(II) chromophores, which display short ^{3}MLCT lifetimes within the microsecond range, are by far more exploited than Cr(III) as sensitizers in polymetallic devices, this mainly because of the complicated and weakly developed synthetic strategies leading to heteroleptic chromium complexes.[BD30] Currently limited to homoleptic complexes, Cr(III)-polypyridyl chromophores have been only sporadically involved as optical partners in polymetallic architectures[BD48,BD49,BD50,BD51] exhibiting light downshifting[BD52] or up-converted emission.[BD32,BD33,BD34,BD35] According that the well-known D_3-symmetrical ter-bidentate [$Cr(bipy)_3$]$^{3+}$ or [$Cr(phen)_3$]$^{3+}$ complexes (i) offer a large array of functionalization possibilities due to the rich bipy

and phen ligand chemistry, (ii) display acceptable metal-centered lifetimes (63 μs ≤ τ ≤ 356 μs) and (iii) may undergo specific ligand substitutions to give heteroleptic derivatives,[BD29,BD41,BD44,BD45,BD46] the target $[Cr(phen)_2(N\text{-}N')]^{3+}$ building blocks emerge as valuable and versatile candidates for working as heteroleptic sensitizers in extended polymetallic structures. However, the remarkable strategy developed by *Kane-Maguire*[BD44,BD45] for the preparation of heteroleptic ter-bidentate chromium complexes does not tolerate electron-withdrawing ligands,[BD44,BD45,BD46] and we are aware of a single recent report, in which this limitation was partially overcome via overheating under microwave radiation.[BD18] To more globally solve this problem, we describe herein a novel versatile synthetic method that permits the synthesis of a complete family of heteroleptic $[Cr(phen)_2(N\text{-}N')]^{3+}$ complexes with few, if any, electronic restrictions. This work then highlights how the variations in ligand-based electronic and geometrical characteristics (Scheme 1) affect the Cr(III) ligand field and nephelauxetic parameters, together with their consequences on the degeneracy and lifetime of the emissive doublet excited state, two parameters which are crucial for further exploitation as sensitizers.

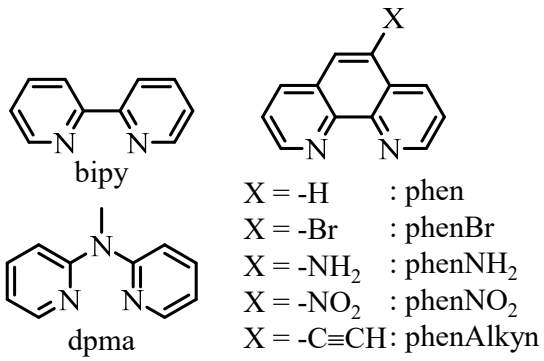

Scheme 1. Chemical structures of the bidentate ligand used in this work.

RESULTS ANS DISCUSSIONS

Synthesis and characterization of heteroleptic ter-bidentate Cr(III) complexes. The first step of the *Kane-Maguire* strategy[BD44,BD61] was successfully reproduced in our hands and gave the starting

material $[Cr(phen)_2Cl_2]Cl$ (**1**), the crystal structure of which was solved and shown in Figure 1 (Figure S1, Table S1,S2,S4 in the Supporting Information).[BD62]

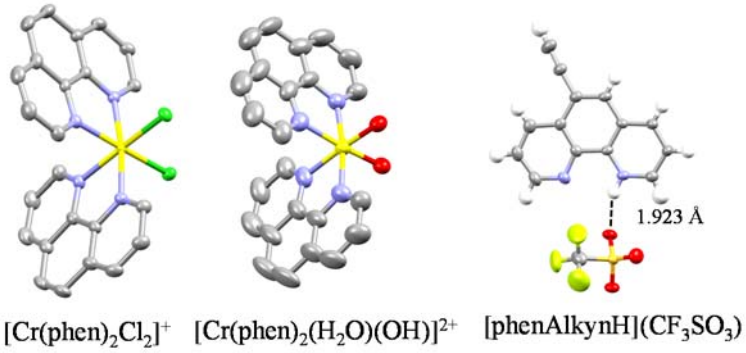

Figure 1. Molecular structures of the cations in the crystal structures of $[Cr(phen)_2Cl_2]Cl\ (CH_3)_2NCHO$ (**1**), $[Cr(phen)_2(H_2O)(OH)](CF_3SO_3)_2$ (**5**) and $[phenAlkynH](CF_3SO_3)$ (**4**) showing H bond length. Color code: Cr (yellow), C (grey), N (blue), O (red), S (orange), F (pale green), Cl (green). Ellipsoids are drawn at 50 % probability. The *Δ* enantiomer is represented for each complex.

Subsequent reaction of $[Cr(phen)_2Cl_2]Cl$ with trifluoromethane sulfonic acid, followed by precipitation in diethylether led to the formation of the key intermediate $[Cr(phen)_2(CF_3SO_3)_2]CF_3SO_3$. Addition of 1,10-phenanthroline (phen), or of 5-bromo-1,10-phenanthroline (phenBr) ultimately yielded, respectively 41 % and 66 % of the target pure homoleptic $[Cr(phen)_3](PF_6)_3$ (**2**, Figure 2; Figure S2 and Tables S1, S3, S5)[BD63,BD88] and heteroleptic $[Cr(phen)_2(phenBr)](PF_6)_3$ (**3**, Figure 2; Figure S5 and Tables S7, S8, S10) complexes after metathesis with hexafluorophosphate anions. The latter synthetic method failed when using 1,10-phenanthroline possessing weak nitrogen donors as found in 5-nitro-phenantroline ($phenNO_2$) or in more delocalized π system as found in 5-ethynyl-1,10-phenanthroline (phenAlkyn). In the latter case, reaction of $[Cr(phen)_2(CF_3SO_3)_2]CF_3SO_3$ with phenAlkyn resulted in the isolation of single crystals of off-white protonated ligand phenAlkynH (**4**, Figure 1; Figure S3 and Tables S6), together with $[Cr(phen)_2(H_2O)(OH)](CF_3SO_3)_2$ complex (**5,** Figure 1; Figure S4 and Tables S6) as red crystals, which suggest the competitive substitution of triflate anions with water molecules.

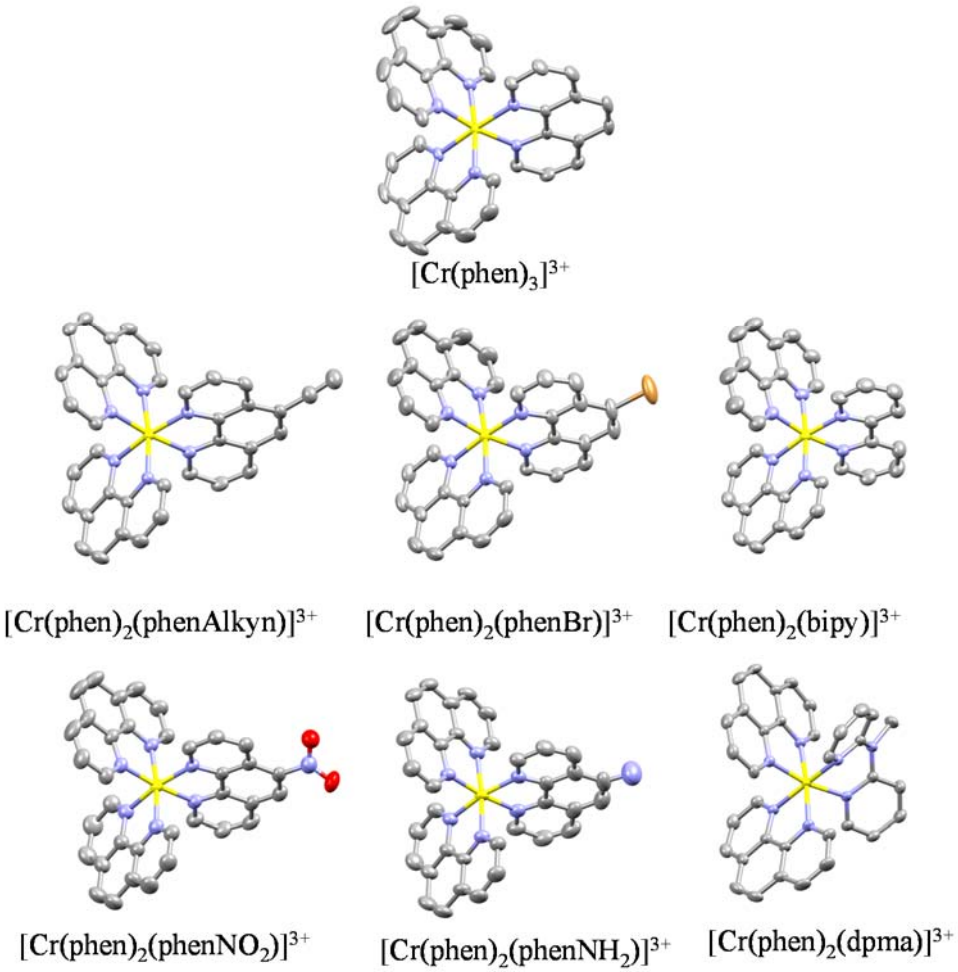

Figure 2. Molecular structures of the cationic complexes in the crystal structures of $[Cr(phen)_3]_2(PF_6)_6$ $6.33CH_3CN$ (**2**), $[Cr(phen)_2(phenBr)](PF_6)_3$ $2CH_3CN$ (**3**), $[Cr(phen)_2(phenAlkyn)](BF_4)_3$ $2CH_3CN$ (**6**), $[Cr(phen)_2(phenNO_2)](CF_3SO_3)_3$ (**7**), $[Cr(phen)_2(phenNH_2)](CF_3SO_3)_3$ $1.83CH_3CN$ (**8**), $[Cr(phen)_2(bipy)](CF_3SO_3)_3$ (**9**) and $[Cr(phen)_2(dpma)](CF_3SO_3)_3$ (**10**). Cr (yellow), C (grey), N (blue), O (red), Br (brown). Ellipsoids are drawn at 50 % probability. Hydrogens and counter-anions are omitted for clarity. The *Δ* enantiomer is represented for each complex.

In order to prevent unwanted ligand protonation and complex hydrolysis, (i) $[Cr(phen)_2Cl_2]Cl$ (**1**) was carefully dried under vacuum, (ii) $[Cr(phen)_2(CF_3SO_3)_2]CF_3SO_3$ was immediately used after synthesis without storage and, last but not least, (iii) a sacrificial base was added during the last step for trapping the excess of trifluoromethane sulfonic acid. Pyridine, but especially sterically-constrained 2,6-lutidine was found to be well-suited for this purpose, since disastrous base-catalyzed Cr(III) complex hydrolysis

could be avoided with these weak bases (Scheme 2).[BD64] It should be highlighted that tremendous ether washing of $[Cr(phen)_2(CF_3SO_3)_2]CF_3SO_3$ intermediate under argon did not permit to avoid the use of sacrificial base.

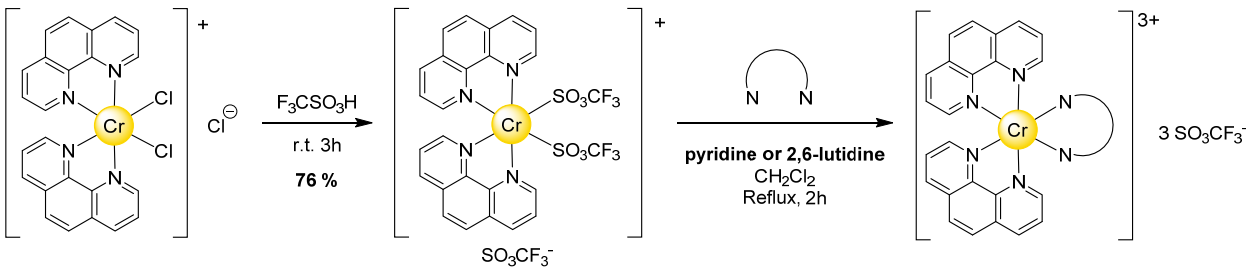

Scheme 2. Versatile synthetic strategy for the preparation of heteroleptic $[Cr(phen)_2(N\text{-}N')]^{3+}$ complexes.

With this modified procedure in hand, $[Cr(phen)_2(phenAlkyn)](BF_4)_3$ (**6**, Figure 2; Figure S6 and Tables S7, S9, S11), $[Cr(phen)_2(phenNO_2)](CF_3SO_3)_3$ (**7**, Figure 2; Figure S7 and Tables S12, S13, S15), $[Cr(phen)_2(phenNH_2)](CF_3SO_3)_3$ (**8**, Figure 2; Figure S8 and Tables S12, S14, S16), $[Cr(phen)_2(bipy)](CF_3SO_3)_3$ (**9**, Figure 2; Figure S9 and Tables S17, S18, S20), $[Cr(phen)_2(dpma)](CF_3SO_3)_3$ (**10**, Figure 2; Figure S10 and Tables S17, S19, S21) were obtained in good yields and without requiring large excess (maximum 2 eq.) of the entering N-N' ligands. All complexes were characterized by elemental analysis, ESI-MS and X-ray-diffraction studies. In all cationic complexes, the three bidentate binding units are wrapped around a pseudo-threefold axis passing through the chromium atom. Both *Λ* and *Δ* enantiomers are present in racemic proportion, which has no impact on the photophysical properties of the mononuclear heteroleptic complexes. However it should be noted that further incorporation into polymetallic architectures might provide complicated mixtures of stereoisomers. Except for $[Cr(phen)_2(dpma)]^{3+}$ in **10**, in which the dpma ligand introduces an unusual six-membered chelate ring, all Cr-N bond lengths (2.045(4)-2.063(4) Å) and chelate N-Cr-N bite angles (80.3(1)-81.1(1)°) are similar, this whatever the substituents bound to the phenanthroline unit.

Altogether, the [CrN_6] chromophores can best be described as pseudo-octahedrons slightly compressed along the pseudo-threefold helical axis (Table S22). As expected,[BD31,BD36,BD54,BD58] the N-Cr-N bite angle in $[Cr(phen)_2(dpma)](CF_3SO_3)_3$ (**10**) is larger for dpma (85.4(1)°, six-membered chelate rings) than for phen ligand (80.0(1)°, five-membered chelate rings). The consequent increased overlap between the donor orbitals of dpma and 3d orbitals of trivalent chromium slightly shortens the Cr-N(dpma) distances (2.045(4) Å) compared with 2.067(4) Å found for the partner phen ligands, Table S22). Neglecting for a while the specific peripheral substitution of the phenanthroline units, all the [CrN_6] chromophores discussed above display local close-to-D_3 symmetry, except $[Cr(phen)_2(dpma)]^{3+}$, for which distortion from threefold symmetry becomes significant.

Photophysical properties of heteroleptic ter-bidentate Cr(III) complexes: **ligand-field strength, nephelauxetic effect and symmetry**.

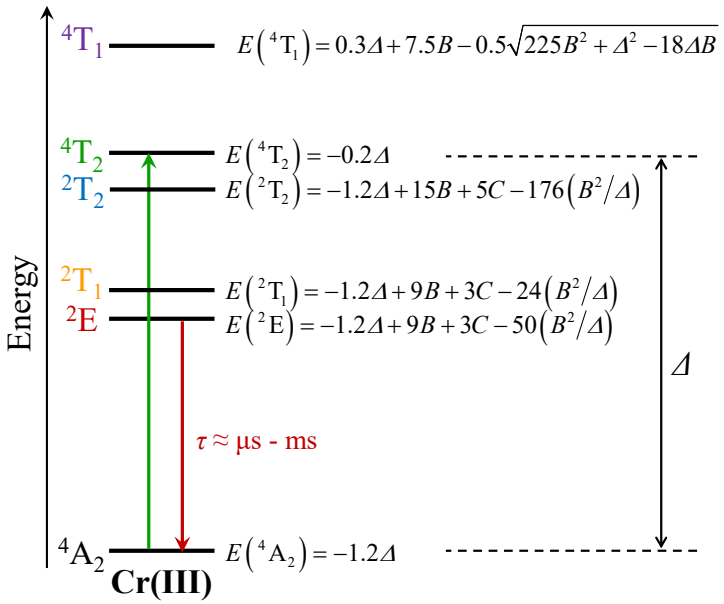

Figure 3. Energy level diagram for [$Cr(III)N_6$] chromophores in octahedral symmetry highlighting the lowest spin-allowed absorption (green arrow), and the lowest spin-forbidden emission (red arrow). The pertinent energy levels can be computed by using ligand field Δ, and Racah parameters B and C.[BD37,BD38]

The keypoint here concerns the unusual large energy gap $\Delta E = \Delta - 9B - 3C + 50\left(B^2/\Delta\right)$ induced between the Cr($^4T_2$) and Cr(^2E) spectroscopic levels in pseudo-octahedral [CrN_6] chromophore, which maximizes Cr($^2E \rightarrow {}^4A_2$) phosphorescence and Cr(^2E) excited state lifetimes *via* the reduced probability of phonon-assisted back intersystem crossing (Figure 3).[BD36] Among a large palette of homoleptic strong-field trivalent chromium complexes,[BD26,BD53] $[Cr(ddpd)_2]^{3+}$ was shown to display the longest room temperature lifetime (898 µs, Figure 4 top),[BD36] which can be further extended by 30 % *via* systematic peripheral deuteration (1.2 ms).[DB54]

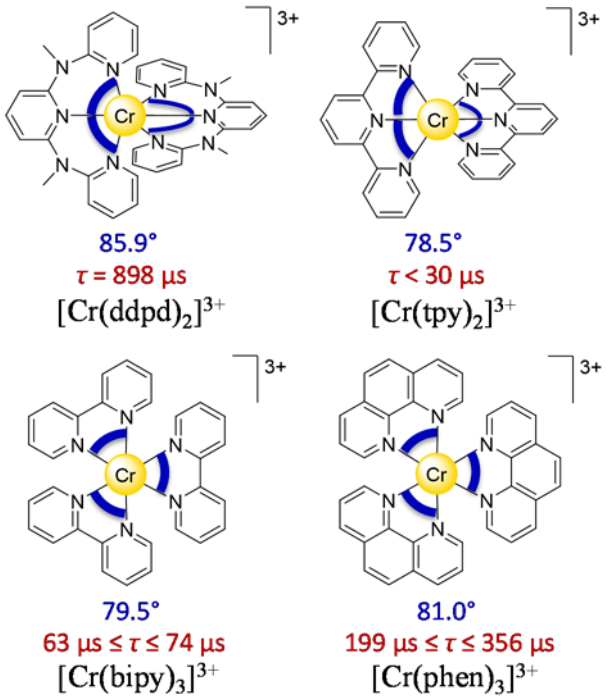

Figure 4. Chemical structures of homoleptic bis-terdentate (top) and ter-bidentate (bottom) chromium complexes where the average N-Cr-N chelate angles (blue), and emissive excited Cr(^2E) lifetimes in solution at room temperature (red) are highlighted.[BD30,BD36,BD56,BD57]

Those impressive features originate from (i) the weak energy of the Cr(^2E) level (12903 cm^{-1}), combined with the strong ligand field induced by minor distortions from local octahedral symmetry which puts the Cr($^4T_2$) level at high energy (22989 cm^{-1}) and (ii) the promotion of ^2E / $^4A_2$ surface

crossing at high energy due to weak distortion from octahedra and anharmonic potential misalignment.[BD55,BD31] The fused six-membered chelate rings produced by the ddpd ligand indeed fix average N-Cr-N chelate angles of 85.9°,[BD36] close to 90° compared with only 78.5° measured for fused five-membered chelate rings found in the analogous $[Cr(tpy)_2]^{3+}$ complex (Figure 4 top).[BD30] The associated short $Cr(^2E)$ lifetime measured for $[Cr(tpy)_2]^{3+}$ ($\tau < 30$ µs) is however much less favorable for its use as an optical sensitizer. Moving toward ter-bidentate $[Cr(bipy)_3]^{3+}$ or $[Cr(phen)_3]^{3+}$ complexes (i) reduces the number of unfavorable constrained 5-membered chelate rings, thus restoring longer metal-centered lifetimes (Figure 4 bottom) [BD56,BD57] and (ii) offer versatile access to Cr(III) complexes due to the rich chemistry of bipy or phen, compared to the weakly developed ddpd functionalization.

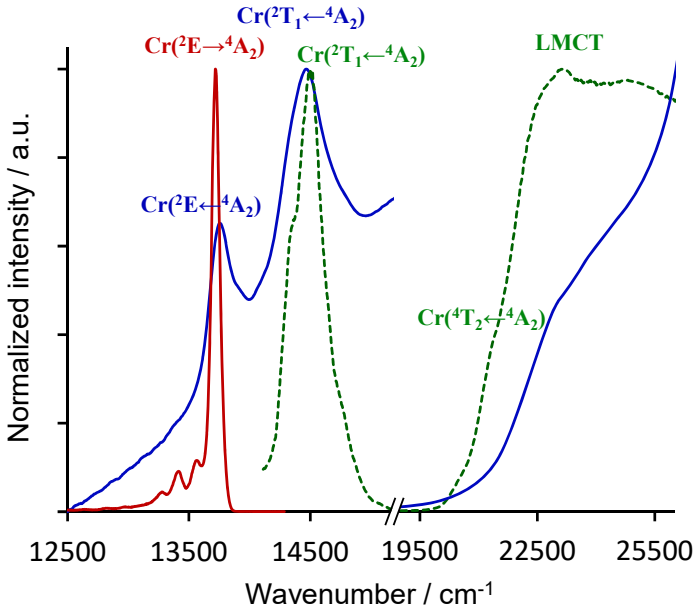

Figure 5. Normalized absorption spectra (full blue traces, solid state (left) and solution (right), 293 K), emission spectrum (λ_{exc} = 355 nm, $\bar{\upsilon}_{exc}$ = 28170 cm^{-1}, red trace, frozen solution acetonitrile/propionitrile (6/4), 10 K) and excitation spectrum (λ_{em} = 731 nm ($\bar{\upsilon}_{em}$ = 13680 cm^{-1}), dashed green line, solid state, 10 K) recorded for $[Cr(phen)_2(phenAlkyn)](BF_4)_3$ (**6**). The spectroscopic labels are those pertinent to idealized octahedral symmetry.

Room-temperature absorption spectra recorded for the CrN_6 complexes **2**, **3**, **6-10** in the solid state and in acetonitrile solution (blue traces in Figure 5, Figures S11-S24) are dominated by weak spin-forbidden Cr(^{2}E←^{4}A$_2$) and Cr(^{2}T$_1$←^{4}A$_2$) transitions at low energy (13500-14500 cm^{-1}, ε < 15 L·mol^{-1}·cm^{-1}), by moderately intense spin-allowed Cr(^{4}T$_2$←^{4}A$_2$) transitions at medium energy (21000-22000 cm^{-1}, ε ≈ 50-500 L·mol^{-1}·cm^{-1}, the spectroscopic labels assume *O* symmetry), by intense ligand-to-metal charge transfer (LMCT) and/or ligand centered ^{4}[^{3}(π*←π)] transitions accompanied with spin-flip in the ^{4}A$_2$ ground state (22000-28000 cm^{-1}, ε ≈ 500-4000 L·mol^{-1}·cm^{-1})[BD85,BD47,BD87] and by ligand-centered π*←π transitions at high energy (> 28000 cm^{-1}; ε ≈ 4000-20000 L·mol^{-1}·cm^{-1}, Table S23). It should be noted that an unambiguous discrimination between the ^{4}[^{3}(π*←π)] and Cr(^{4}T$_2$←^{4}A$_2$) transition is complicated, but (i) the lack of band structuration and (ii) their weak intensity (ε < 300 L·mol^{-1}·cm^{-1}) suggest assignment to ligand-field transitions.[BD85,BD87] UV excitation into the ligand-centered absorption bands (λ_{exc} = 355 nm, $\bar{\upsilon}_{exc}$ = 28170 cm^{-1}) provide low-temperature emission spectra with a single band (accompanied by vibrational progression at lower energy) assigned to the famous near infra-red spin-flip Cr(^{2}E→^{4}A$_2$) luminescence (red trace in Figure 5, Figures S25 and Table S24). At room temperature, thermal equilibrium between the ^{2}T$_1$ and ^{2}E states results in dual Cr(^{2}T$_1$→^{4}A$_2$) and Cr(^{2}E→^{4}A$_2$) phosphorescence (Figure S26 and Table S25),[BD65] a phenomenon corroborated by excitation spectra recorded upon analyzing the Cr(^{2}E→^{4}A$_2$) emissions, which demonstrate efficient sensitization originating from the close Cr(^{2}T$_1$) level (green trace in Figure 5, Figures S27-S33 and Table S26). For all $[CrN_6]$ complexes displaying D_3-symmetry, the Cr(^{2}T$_1$←^{4}A$_2$) transition is split into two components (see the low-energy part of the green trace in Figure 5), which is diagnostic for a noticeable deviation from pure *O* symmetry in the $[CrN_6]$ chromophores. According to Endicott,[BD55] the drop in symmetry induced by the constrained chelate bite angles (transforming O_h into D_3 point groups, see previous section) results in the splitting of the t_{2g} orbitals (O_h symmetry) into a_1+e orbitals

(D_3 symmetry) separated by a small energy gap. The inter-electronic repulsions accompanying the filling of these orbitals with three electrons in Cr(III) complexes produce four spectroscopic levels: a Cr(^{4}E) spin quartet ground state, a low-energy doubly-degenerate doublet Cr(^{2}E) excited level, reminiscent to that found in *O* symmetry and two higher-energy doublet Cr(^{2}A$_2$) + Cr(^{2}E) levels, reminiscent to the Cr(^{2}T$_1$) level found in *O* symmetry. This explains the observation of three spin-flip absorption bands: two Cr(^{2}E←^{4}E) (arising from Cr(^{2}T$_1$←^{4}A$_2$) and Cr(^{2}E←^{4}A$_2$) in *O* point group) and one Cr(^{2}A$_2$←^{4}E) (arising from Cr(^{2}T$_1$←^{4}A$_2$) in *O* point group) for [CrN$_6$] complexes in D_3-symmetry (Figure 5, low-energy blue trace).[BD55] Moreover, the energy gap between the half-occupied Cr-centered a$_1$+e orbitals produces some changes in the bonding parameters between the spin-flip excited states and the ground state.[BD55] The consequent shift in the nuclear coordinates is accompanied by minor, but non-negligible Stokes shifts (≤ 38 cm^{-1}; 2 nm) together with vibronic progressions for the Cr(^{2}E→^{4}E) (Cr(^{2}E→^{4}A$_2$) in *O* point group) emission bands as observed in [Cr(phen)$_3$](PF$_6$)$_3$ (**2**), [Cr(phen)$_2$(phenBr)](PF$_6$)$_3$ (**3**), [Cr(phen)$_2$(phenAlkyn)](BF$_4$)$_3$ (**6**), [Cr(phen)$_2$(phenNO$_2$)](CF$_3$SO$_3$)$_3$ (**7**), [Cr(phen)$_2$(phenNH$_2$)](CF$_3$SO$_3$)$_3$ (**8**), [Cr(phen)$_2$(bipy)](BF$_4$)$_3$ (**9**), (Figure 5 and Figures S11-S25). A detailed analysis of the vibronic progression using an anharmonic *Morse* potentials for modelling the energy gap $\Delta E = E(V+1)–E(V)$ between two adjacent vibrational levels of the ground state (ν_0 is the fundamental frequency and D the ground state dissociation energy), is summarized in eq. (2).[BD66]

$$\Delta E = E(V+1) - E(V) = h\nu_0 - (V+1)\frac{(h\nu_0)^2}{2D} \qquad (2)$$

Plots of $\Delta E = E(V+1)–E(V)$ as a function of V+1 indeed gave straight lines (Figure S34), from which $855 \leq D \leq 1920$ cm^{-1} and $163 \leq \nu_0/c \leq 182$ cm^{-1} can be calculated for the ground state (Table S27).[BD66] The vibronic progression induced by the release in symmetry involves Cr-N stretching modes (163-182 cm^{-1}), which altogether spread the Cr(^{2}E→^{4}E) (Cr(^{2}E→^{4}A$_2$) in *O* point group) emission band over 600

cm^{-1}. This represents a considerable advantage for maximizing the spectral overlap integrals $J(\lambda)$ between the Cr(III)-based sensitizer and nearby activators (eq. 1). $[Cr(phen)_2(dpma)](CF_3SO_3)_3$ (**10**) undergoes a further drop in symmetry because the $[CrN_6]$ coordination sphere is now close to C_2-symmetry. Within this point group, only mono-dimensional irreducible representations are available and the orbital degeneracies of the spin-flip $Cr(^2T_1 \leftrightarrow {}^4A_2)$ and $Cr(^2E \leftrightarrow {}^4A_2)$ transitions in *O* symmetry are completely lifted. We therefore expect, and observe two groups of absorption in the NIR domain for $[Cr(phen)_2(dpma)]^{3+}$ with three (originating from the T term), respectively two (originating from the E term) components (Figure 6). The splitting of the $Cr(^2E)$ level is corroborated by the detection of dual NIR emission at 293K (Figure S26). As matter of clarity, throughout the rest of the study the *O* point group will be assumed for labelling energy levels.

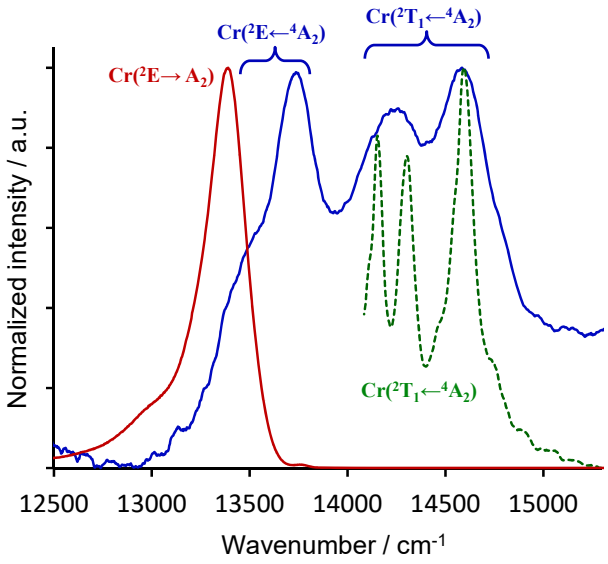

Figure 6. Normalized absorption spectrum (blue trace, solid state at 293 K), emission spectrum (red trace, frozen solution acetonitrile/propionitrile (6/4) at 10 K, λ_{exc} = 355 nm, $\bar{\upsilon}_{exc}$ = 28169 cm^{-1}) and excitation spectrum (dashed green trace, solid state at 10 K, λ_{em} = 747 nm, $\bar{\upsilon}_{em}$ = 13387 cm^{-1}) recorded for $[Cr(phen)_2(dpma)](CF_3SO_3)_3$ (**10**). The spectroscopic labels are those pertinent to idealized octahedral symmetry.

As a consequence of the symmetry release, the global near-infrared emission of $[Cr(phen)_2(dpma)](CF_3SO_3)_3$ (**10**) is spread over 1300 cm^{-1} at 10 K, which makes this complex the most versatile candidate for optimizing spectral overlap between Cr(III) sensitizer and potential activators. The combination of the approximate equations gathered in Figure 3[BD37,BD38] with the experimentally accessible energies found for the $Cr(^4T_2)$, $Cr(^2T_1)$, and $Cr(^2E)$ levels (relative to the $Cr(^4A_2)$ ground state taken as a reference) provide (i) estimations for the ligand field Δ, and Racah parameters *B* and *C* (Table 1) together with (ii) predictions for the energies of the missing metal-centered energy levels $Cr(^2T_2)$ and $Cr(^4T_1)$ (Figure 7, these approximate calculations assume *O* point group).

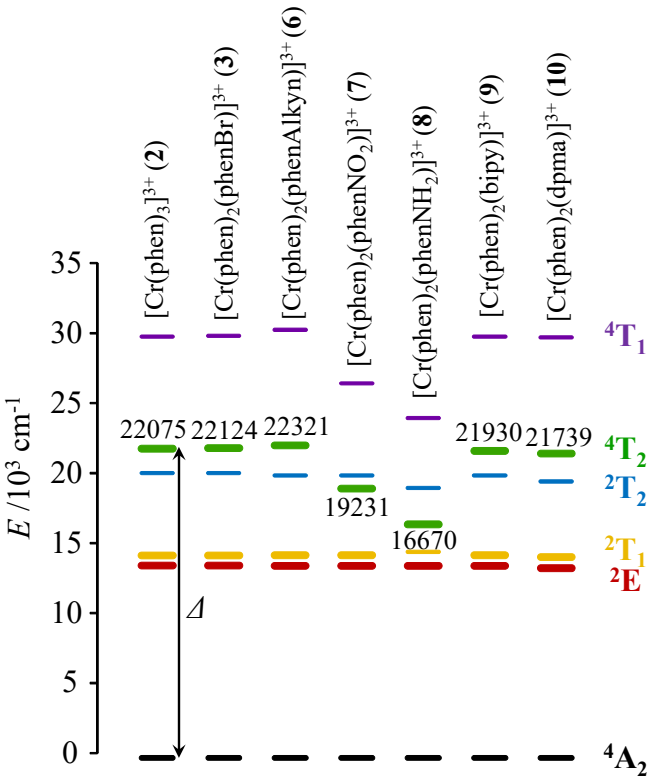

Figure 7. Energy level diagram for $[Cr(phen)_2(N\text{-}N')]^{3+}$ complexes, showing low-energy metal-centered levels (experimentally determined: thick trace; calculated: thin trace).

Table 1. Ligand fields Δ and Racah parameters B and C for pseudo-octahedral $[Cr(phen)_2(N\text{-}N')]^{3+}$ complexes deduced by using the equations gathered in Fig.1 and the experimental Cr-centered ^2E, $^2T_1$, $^4T_2$ energies.[a] The energies of $Cr(^2T_2)$ and $Cr(^4T_1)$ are computed (italic fonts).

Complex	$\sigma_I^{N-N'}$ [b]	$\sigma_R^{N-N'}$ [c]	Δ /cm^{-1}	B /cm^{-1}	C /cm^{-1}	Δ/B	C/B	E / cm^{-1} [d]				
								^2E	$^2T_1$	$^4T_2$	$^2T_2$	$^4T_1$
$[Cr(phen)_3]^{3+}$ (**2**)	0	0	22075	779	2700	28	3.5	13736	14451	22075	*20347*	*30090*
$[Cr(phen)_2(phenBr)]^{3+}$ (**3**)	0.47	-0.16	22124	780	2697	28	3.5	13736	14451	22124	*20347*	*30150*
$[Cr(phen)_2(phenAlkyn)]^{3+}$(**6**)	0.29	0.08	22321	805	2642	28	3.3	13717	14472	22321	*20174*	*30565*
$[Cr(phen)_2(phenNO_2)]^{3+}$ (**7**)	0.67	0.16	19231	747	2815	26	3.8	13717	14472	19231	*20174*	*26754*
$[Cr(phen)_2(phenNH_2)]^{3+}$ (**8**)[e]	0.17	-0.48	16670	803	2809	21	*3.5*[e]	13717	*14722*[e]	16670	*19281*	*24275*
$[Cr(phen)_2(bipy)]^{3+}$ (**9**)	-	-	21930	798	2663	27	3.3	13717	14472	21930	*20174*	*30085*
$[Cr(phen)_2(dpma)]^{3+}$ (**10**)	-		21739	816	2579	27	3.2	13550	14347	21739	*19743*	*30027*

[a] The spectroscopic labels refer to pure O symmetry. For $[Cr(phen)_2(dpma)](CF_3SO_3)_3$ (**10**), the energies of parent $Cr(^2T_1)$ and $Cr(^2E)$ levels were taken as the energy averages of their various components (see text). [b] Hammett parameter estimating the inductive electronic effects of the substituent on the *N-N*' phenanthroline σ orbitals.[BD67] [c] Hammett parameter estimating the resonance electronic effects of the substituent on the *N-N*' phenanthroline π orbitals.[BD67] [d] energies are given with respect to $Cr(^4A_2)$ ground state. [e] $Cr(^2T_1 \leftarrow {}^4A_2)$ was masked by LMCT bands. The ligand field Δ and Racah parameter B were determined assuming $C = 3.5B$,

In absence of strong electron-withdrawing (-NO_2) or electron-donating (-NH_2) substituents, all heteroleptic $[Cr(phen)_2(N\text{-}N')]^{3+}$ complexes display similar ligand-fields ($\Delta \approx 22000$ cm^{-1}, Figure 7) and nephelauxetic effects ($B \approx 800$ cm^{-1}, Table 1) in agreement with the only minor structural variations found for these $[CrN_6]$ coordination units in their crystal structures. As expected, the strong inductive (Hammett coefficient $\sigma_I(NO_2) = 0.67$) and resonance (Hammett coefficient $\sigma_R(NO_2) = 0.16$) electron-withdrawing nitro group, when connected to one phenanthroline unit in $[Cr(phen)_2(phenNO_2)](CF_3SO_3)_3$ (**7**), weakens the ligand field (Δ decreases) and reinforces the nephelauxetic effect (B decreases). As rather naive chemists, we originally expected that the connection of the opposite electron-donating amino group in $[Cr(phen)_2(phenNH_2)](CF_3SO_3)_3$ (**8**) should result in the opposite trend. However, Hammett coefficients teach chemists that amino substituents, because of the presence of electronegative nitrogen atoms, are indeed (poor) σ-acceptors ($\sigma_I(NH_2) = 0.17$), while donation concerns only π effects ($\sigma_R(NH_2) = -0.48$).[BD67] With this in mind, some efficient π-overlap between filled $phenNH_2$ orbitals and $Cr(t_{2g})$ orbitals is expected to reduce Δ, while electron delocalization is simultaneously restricted to yield large Racah parameter B, a prediction in agreement with experimental data summarized in Figure 7. In addition to the detrimental N-H high-frequency multiphonon relaxation,[BD75,BD27,BD76,BD86] the reduced $Cr(^4T_2)$-$Cr(^2E)$ energy gap in $[Cr(phen)_2(phenNH_2)]^{3+}$ favors back inter-system crossing (BISC), two characteristics which limit metal-centered phosphorescence as previously documented for analogous non-emissive bis-terpyridine Cr(III) complexes bearing amino group.[BD47]

Emissive properties of heteroleptic ter-bidentate Cr(III) complexes: **excited-state lifetimes**. Time-resolved emissions demonstrate that the $Cr(^2E)$ emission lifetimes measured in heteroleptic $[Cr(phen)_2(N\text{-}N')]^{3+}$ complexes strongly depend on temperature (Figure 8 and Tables S28-29). Beyond spontaneous radiative relaxation responsible for photon emission and modeled with the temperature-

independent *Einstein*'s law,[BD68,BD69,BD70] competitive non-radiative Cr(^{2}E) depopulation can be induced by temperature-dependent phonon-assisted pathways such as (i) weak coupling with vibration modes that requires weak activation energy and persist at low temperature,[BD26] (ii) crossing with a photochemical intermediate in its ground electronic state (GSI),[BD26,BD27] (iii) release of symmetry that induces anharmonic potential misalignment and the appearance of surface crossing between ^{2}E and ^{4}A$_2$ states,[BD27,BD55] (iv) surface crossing due to trigonal distortion in excited ^{2}E state induced by ligand steric strain relief[BD27,BD71] and (v) back inter-system crossing (BISC) from ^{2}E to ^{4}T$_2$ state, which is evidenced by non-exponential decay.[BD26,BD72] The latter mechanism is only significant for ^{2}E–^{4}T$_2$ gap weaker than 3400 cm^{-1} as found in [CrN$_4$O$_2$] complexes, and should be overpassed for most of our [CrN$_6$] complexes.[BD26,BD28,BD72,BD73]

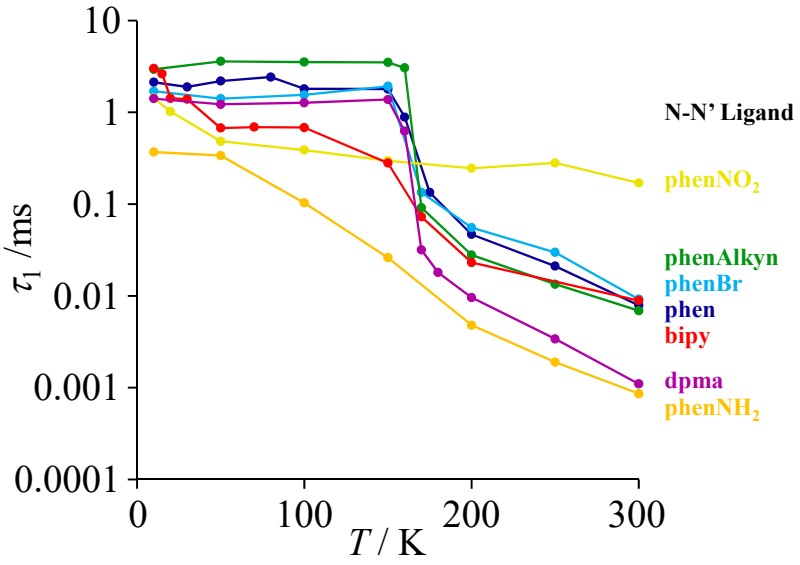

Figure 8. Temperature-dependent Cr(^{2}E) emission lifetimes (τ_1) measured in mixture acetonitrile/propionitrile (6/4) (5×10^{-3} mol·L^{-1}), of [Cr(phen)$_3$](PF$_6$)$_3$ (**2**) (dark blue), [Cr(phen)$_2$(phenBr)](PF$_6$)$_3$ (**3**) (light blue), [Cr(phen)$_2$(phenAlkyn)](BF$_4$)$_3$ (**6**) (green), [Cr(phen)$_2$(phenNO$_2$)](CF$_3$SO$_3$)$_3$ (**7**) (yellow, measured on powder samples since degradation occurred in propionitrile), [Cr(phen)$_2$(phenNH$_2$)](CF$_3$SO$_3$)$_3$ (**8**) (orange), [Cr(phen)$_2$(bipy)](BF$_4$)$_3$ (**9**) (red), [Cr(phen)$_2$(dpma)](CF$_3$SO$_3$)$_3$ (**10**) (purple).

The Cr(^{2}E) emission decays were measured in air equilibrated acetonitrile/propionitrile (6/4) solution from 10 K to 300 K (Figure S35–S45), and in degazed acetonitrile solution at 293 K (Figure S46) for the $[Cr(phen)_2(N\text{-}N')]^{3+}$ complexes. From 10 K to 150 K, the decay curves could be fitted with double exponential laws due to the formation of aggregates upon freezing, in which intermolecular energy transfers resulted in self-quenching and bi-exponential decays.[BD74,BD40] Upon melting around 150 K, mono-exponential decays were recovered in agreement with the existence of isolated solvated Cr(III) complexes. The double exponential fit observed in frozen solution can be thus partitioned between a short lifetime (τ_2), assigned to partially-quenched Cr(^{2}E) levels found in aggregates, and a long lifetime (τ_1) assigned to Cr(^{2}E) levels in isolated complexes (Table S28). The $[Cr(phen)_2(phenNH_2)]^{3+}$ complex systematically exhibits the shortest Cr(^{2}E) lifetimes of the series at any temperature (orange trace in Figure 8), du to combined effect of (i) a reversible Cr(^{2}E)↔Cr($^4T_2$) back-intersystem crossing produced by the weak ligand field in this complex (Figure 7) since the energy gap $\Delta E(^2E–^4T_2)$ = 2950 cm^{-1} is below the upper limit of 3400 cm^{-1} set by Forster,[BD26,BD72] and (ii) the presence of unfavorable high-energy N-H oscillators, which are famous for quenching the Cr(^{2}E) level.[BD75,BD27,BD76,BD86] While BISC is phonon assisted and predominant at high temperature, the presence of N-H vibration modes open a de-excitation pathway that requires weak thermal activation and persist at low temperature. All the other $[Cr(phen)_2(N\text{-}N')]^{3+}$ complexes possess roughly constant Cr(^{2}E) lifetimes in the millisecond range from 10 K to 150 K in frozen solutions, which suggests the predominance of the radiative rate constant for the de-excitation of the Cr(^{2}E) level at these temperatures. Upon melting around 150 K, an abrupt decrease of τ_1 results from the emergence of coupling processes with solvent vibrational modes and the operation of thermally-activated relaxation processes. However this abrupt decrease is not observed for $[Cr(phen)_2(phenNH_2)]^{3+}$, probably because the deleterious effect of N-H vibration dominates the desexcitation processes and remains predominant upon solution melting regarding

additional quenching processes produced by the diffusion of O_2. At room temperature in oxygen-free acetonitrile, the decays of the $Cr(^2E)$ levels in $[Cr(phen)_2(N\text{-}N')]^{3+}$ complexes are mono-exponential (except N-N' = $phenNH_2$, Figure 9). They amount to about 200 μs, apart from $[Cr(phen)_2(phenNH_2)]^{3+}$ and $[Cr(phen)_2(dpma)]^{3+}$ which show lifetime two orders of magnitude smaller than those found at 10 K (Table 2).

Table 2. $Cr(^2E)$ emission lifetimes (τ_1) for heteroleptic $[Cr(phen)_2(N\text{-}N')]^{3+}$ complexes.

Complex	T / K	τ_1 / μs
$[Cr(phen)_3](PF_6)_3$ (**2**)	10 [a]	2100
	293 [b]	224
$[Cr(phen)_2(phenBr)](PF_6)_3$ (**3**)	10 [a]	1700
	293 [b]	214
$[Cr(phen)_2(phenAlkyn)](BF_4)_3$ (**6**)	10 [a]	2900
	293 [b]	259
$[Cr(phen)_2(phenNO_2)](CF_3SO_3)_3$ (**7**)	10 [c]	1400
	293 [b]	177
$[Cr(phen)_2(phenNH_2)](CF_3SO_3)_3$ (**8**)	10 [a]	370
	293 [b]	17
$[Cr(phen)_2(bipy)](BF_4)_3$ (**9**)	10 [a]	3000
	208 [b]	208
$[Cr(phen)_2(dpma)](CF_3SO_3)_3$ (**10**)	10 [a]	1400
	293 [b]	23

[a] Lifetimes measured in air equilibrated frozen acetonitrile/propionitrile (6/4) solutions ($C = 5\times10^{-3}$ mol/L). [b] Lifetimes measured in freeze pump thaw degassed acetonitrile solution ($C = 10^{-4}$ mol/L). [c] lifetime measured in solid state.

A close scrutiny at Figure 8, shows that $[Cr(phen)_2(bipy)](BF_4)_3$ (**9**) and $[Cr(phen)_2(dpma)](CF_3SO_3)_3$ (**10**) display maximum drops in lifetime in the 10-293 K range due to the additional rotational degrees of freedom found in bipy and dpma, compared with phen. This provides extra vibration modes for both

complexes[BD76] and larger anharmonic potential misalignment and surface crossing for $[Cr(phen)_2(dpma)]^{3+}$ justifying its particularly short lifetime (23 µs, Table 2) at 293 K in O_2-free solution.[BD55,BD71,BD27] Finally, $[Cr(phen)_2(phenAlkyn)](BF_4)_3$ (**6**) display the longest lifetime in frozen solution below 150 K (around 3 ms), that remains non-negligible at room temperature in degassed solution (259 µs).

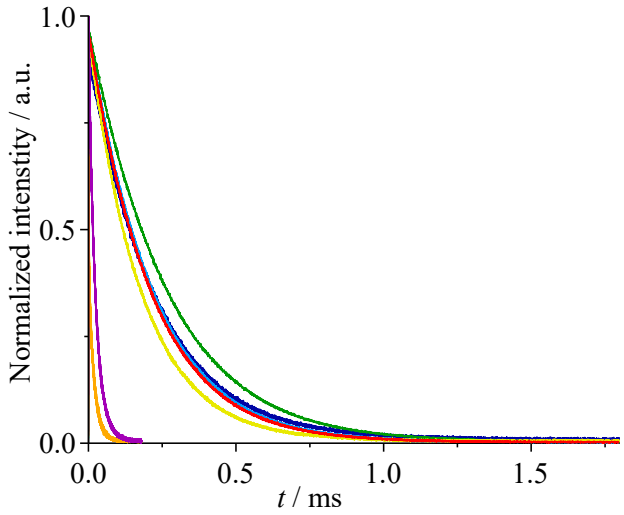

Figure 9. $Cr(^2E)$ emission decay curves measured in freeze pump thaw degassed acetonitrile (293 K, 10^{-4} mol·L^{-1}, λ_{exc} = 355 nm) for $[Cr(phen)_3](PF_6)_3$ (**2**, dark blue), $[Cr(phen)_2(phenBr)](PF_6)_3$ (**3**, light blue), $[Cr(phen)_2(phenAlkyn)](BF_4)_3$ (**6**, green), $[Cr(phen)_2(phenNO_2)](CF_3SO_3)_3$ (**7**, yellow), $[Cr(phen)_2(phenNH_2)](CF_3SO_3)_3$ (**8**, orange), $[Cr(phen)_2(bipy)](BF_4)_3$ (**9**, red), $[Cr(phen)_2(dpma)](CF_3SO_3)_3$ (**10**, purple).

CONCLUSION

The use of non-coordinating and weakly basic 2,6-lutidine as a sacrificial base for trapping excess of acid extends the *Kane-Maguire* synthetic strategy to the preparation of kinetically-inert heteroleptic ter-bidentate Cr(III) complexes $[Cr(phen)_2(N\text{-}N')]^{3+}$, which may include electron-withdrawing or electron-donating bidentate ligands. Building on this success, both electronic properties and symmetry effects

can be rationally implemented into [CrN_6] chromophores for tuning their optical properties. Firstly, pseudo-D_3 symmetry can be taken as a satisfying model for the analysis of both the coordination spheres (octahedrons compressed along the pseudo-threefold axis) and the luminescence properties (two bands for the Cr($^2T_1 \rightarrow {}^4A_2$) and one band for the Cr($^2T_1 \rightarrow {}^4A_2$) spin-flip transitions derived from *O* symmetry) in $[Cr(phen)_2(N\text{-}N')]^{3+}$. Secondly, the co-existence of five-membered and six-membered chelate rings in $[Cr(phen)_2(dpma)]^{3+}$ induces further deviation from trigonal symmetry, which significantly broadens the spectral domain covered by the NIR emission, an advantage for spectral overlap with low-energy acceptors obtained at the cost of additional non-radiative relaxation processes. Despite short room temperature Cr(^2E) lifetime, the combination of long Cr(^2E) lifetime (1.4 ms) and large spectral width at 10 K, makes $[Cr(phen)_2(dpma)]^{3+}$ compatible with sensitization in these specific conditions. With this in mind, $[Cr(phen)_2(phenAlkyn)]^{3+}$ finally emerges as the best and most versatile candidate for being selected as sensitizer in Cr-based optically-active metallo-supramolecular assemblies. At 10 K, this complex possesses a long Cr^{III}(^2E) lifetime (2.9 ms) together with reasonably large spectral NIR emission (spread over 600 cm^{-1}). At room temperature, its excited-state lifetime in deoxygenated solution remains long enough (259 μs) for being exploited as relay and the synthetic versatility of its C-C triple bond is compatible with its connections to neighboring activators.[BD30]

EXPERIMENTAL SECTION

General procedures. ^1H and ^{13}C NMR spectra were recorded on a *Bruker Avance* 400 MHz spectrometer equipped with a variable temperature unit. Chemical shifts were given in ppm with respect to tetramethylsilane $Si(CH_3)_4$. Pneumatically-assisted electrospray (ESI) mass spectra were recorded from 10^{-4} M solutions on an Applied Biosystems API 150EX LC/MS System equipped with a Turbo Ionspray source®. Elemental analyses were performed by K. L. Buchwalder from the Microchemical Laboratory of the University of Geneva. Reagent grade tetrahydrofuran and diethyl

ether were distilled from sodium and benzophenone. Reagent grade dichloromethane was distilled from CaH_2. 5-nitrophenathroline (phenNO_2),[BD77] 5-aminophenathroline (phenNH_2)[BD77] and Di(pyrid-2-yl)(methyl)amine) (dpma)[BD78] were synthetized according to literature procedures. All other chemical were purchased from commercial sources and used without further purification. Silica-gel plates (Merck, 60 F_{254}) were used for thin-layer chromatography. Preparative column chromatography was performed using either neutral alumina gel from Fluka (Typ 507 C) 100-125 mesh or SiliaFlash® silica gel P60 (0.04-0.063 mm).

Preparation of 5-bromo-1,10-phenanthroline.[BD79] 1,10-phenanthroline (7 g, 38.9 mmol, 1 eq) was loaded in a heavy walled glass reaction tube equipped with a Teflon screw top fitted with a Viton O-ring. The vessel was put into an ice bath and oleum (22-30%, 25 mL) and bromine (0.95 mL, 2.95 g, 18.4 mmol, 0.47 eq) were added. The mixture was heated and stirred at 135°C for 16 h. The solution was cooled to room temperature, poured into ice and neutralized with KOH. The excess bromine was destroyed with sodium thiosulfate. The mixture was extracted three times with dichloromethane (3 × 200 mL). The combined organic phase were washed twice with water (2 × 300 mL), dried over $MgSO_4$, filtered, and evaporated to dryness, providing 8.72 g of crude product. The solid was dissolved in minimum of dichloromethane, then Et_2O was added until the solution turned turbid. The flask was closed and the mixture let to crystallize overnight. The resulting solid was collected by filtration (5.51 g), and re-crystallized using the same procedure to yield pure 5-bromo-1,10-phenanthroline (4.24 g, 42 %).

^{1}H NMR (400 MHz, $CDCl_3$) δ 9.22 (m, 2H), 8.68 (dd, J = 8.4, 1.6 Hz, 1H), 8.20 (dd, J = 8.1, 1.8 Hz, 1H), 8.17 (s, 1H), 7.76 (dd, J = 8.4, 4.4 Hz, 1H), 7.66 (dd, J = 8.1, 4.3 Hz, 1H). ^{13}C NMR (100 MHz, $CDCl_3$): δ 150.7, 150.5, 146.5, 145.5, 135.7, 134.9, 129.5, 128.6, 127.7, 123.6, 123.5, 120.6. ESI-MS *m/z*: $[M + H]^+$ ($C_{12}H_8BrN_2$): 259.3, 261.3.

Preparation of 5-ethynyl-1,10-phenanthroline. 5-bromo-1,10-phenanthroline (4.0 g, 15.4 mmol, 1 eq), $PdCl_2(PPh_3)_2$ (867 mg, 1.24 mmol, 8 mol%), CuI (472 mg, 2.48 mmol, 16 mol%), and a mixture of NEt_3 (28 mL)/THF (56 mL) previously degassed by argon bubbling (30 min) were introduced into a Schlenk tube under argon. Trimethylsilyacetylene (TMSA, 5.35 mL, 3.79 g, 38.5 mmol, 2.5 eq) was then added. The mixture was stirred at 75°C for 16 hours. After solvent evaporation, the crude product was dissolved in dichloromethane (150 mL) and 4 mL of tris(2-aminoethyl)amine were added until the solution turned greenish blue. The organic layer was diluted to 500 mL, washed by water (4 × 300 mL), dried over anhydrous $MgSO_4$, filtered, and the solvent was evaporated. The resulting crude was purified by plug filtration (Al_2O_3: CH_2Cl_2/MeOH (0-3%)) providing 4.5 g of intermediate 5-[(trimethylsilyl)ethynyl]-1,10-phenanthroline. The latter compound was introduced into a round bottom flask, dissolved in CH_2Cl_2 (50 mL) and completed with a solution of tetrabutylammonium fluoride (TBAF 1 mol/L in THF, 21.2 mL, 21.2mmol, 1.3 eq). The mixture was stirred at room temperature for 15 min, then diluted in CH_2Cl_2 (400 mL) and washed by water (4 × 300 mL) to afford 2.58 g of crude product. Purification by column chromatography (Al_2O_3: CH_2Cl_2/Acetone (0-50%)), followed by trituration and stirring of the final solid during 2h in Et_2O (25 mL) yielded pure 5-ethynyl-1,10-phenanthroline (1.428 g, 7.0 mmol, 45 %) as an off-white solid. ^{1}H NMR (400 MHz, $CDCl_3$) δ 9.23 (dd, J = 4.3, 1.7 Hz, 1H), 9.21 (dd, J = 4.4, 1.7 Hz, 1H), 8.77 (dd, J = 8.2, 1.7 Hz, 1H), 8.23 (dd, J = 8.1, 1.7 Hz, 1H), 8.09 (s, 1H), 7.73 (dd, J = 8.3, 4.3 Hz, 1H), 7.66 (dd, J = 8.1, 4.4 Hz, 1H), 3.55 (s, 1H). ^{13}C NMR (100 MHz, $CDCl_3$): δ 151.3, 150.9, 146.5, 146.0, 136.0, 134.7, 131.9, 128.4, 127.9, 123.6, 123.5, 119.0, 83.3, 80.2. ESI-MS *m/z*: $[M + H]^+$ ($C_{14}H_9N_2$): 204.4; $[2M + H]^+$ ($C_{28}H_{17}N_4$): 409.1.

Preparation of $[Cr(phen)_2Cl_2]Cl$ (1).[BD80] $CrCl_3$ anhydrous (0.56 g, 3.55 mmol, 1eq), 1,10-phenanthroline (2.00 g, 11.13 mmol, 3.1 eq), and absolute ethanol (20 mL) were introduced into a round bottom flask. The mixture was heated to reflux and three tablets of zinc (1.2 g) were added. The mixture was heated to reflux during 10 min. The produced green solid was filtered over a ptfe

membrane and dried with Et_2O. Removal of excess of Zn tabs with tweezers afforded 93 % (1.71 g) of $[Cr(phen)_2Cl_2]Cl$ as a green powder. Elemental analysis calc (%) for $Cr(phen)_2Cl_2]Cl\cdot 1.2H_2O\cdot 1.5EtOH$: C 53.21, H 4.53, N 9.19; found: C 53.26, H 4.33, N 9.00. Slow diffusion of Et_2O into a solution of $[Cr(phen)_2Cl_2]Cl$ in DMF provided green single crystals suitable for XRD.

Preparation of $[Cr(phen)_2(CF_3SO_3)_2](CF_3SO_3)$.[BD61,BD29,BD44] Trifluoromethanesulfonic acid (7mL) was added to $[Cr(phen)_2Cl_2]Cl$ (1.5 g, 2.89 mmol) into a Schlenk tube under argon and heated at 100°C for two hours with argon bubbling. The solution was cooled on ice and vigorously stirred. Anhydrous distilled diethyl ether (40mL) was added and led to the formation of a pink precipitate. The solid was filtered under argon , washed twice with anhydrous diethyl ether and transferred into the glove box where the pink precipitate was stored $[Cr(phen)_2(CF_3SO_3)_2](CF_3SO_3)$ (2.51 g, 2.49 mmol, yield 86%). ESI-MS *m/z*: $[Cr(phen)_2(CF_3SO_3)_2]^+$ 710.4. Elemental analysis calc (%) for $[Cr(phen)_2(CF_3SO_3)_2](CF_3SO_3)\cdot 1.1\ HSO_3CF_3$: C 32.94, H 1.68, N 5.47; found: C 33.22, H 1.85, N 5.25.

Preparation of $[Cr(phen)_3](PF_6)_3$ (2). $[Cr(phen)_2(CF_3SO_3)_2](CF_3SO_3)$ (200 mg, 0.232 mmol, 1 eq), 1,10-phenanthroline (126 mg, 0.636 mmol, 2.7 eq), and anhydrous distilled dichloromethane (15 mL) were introduced into a Schlenk tube under argon. The reaction mixture was heated at 45°C for 90 min. The resulting yellow solid was filtered on a ptfe membrane, washed with CH_2Cl_2 and dried with diethyl ether to give pure $[Cr(phen)_3](CF_3SO_3)_3$ (98 mg, 0.094 mmol, yield 41%). Metathesis resulted from the dissolution of $[Cr(phen)_3](CF_3SO_3)_3$ in a minimum amount of MeOH, followed by the addition of a saturated solution of $TBAPF_6$ in MeOH. The resulting precipitate of $[Cr(phen)_3](PF_6)_3$ was filtered and dried. Slow diffusion of Et_2O into a solution of $[Cr(phen)_3](PF_6)_3$ in acetonitrile provided single crystals suitable for XRD. ESI-MS *m/z*: $[[Cr(phen)_3](CF_3SO_3)_2]^+$ 890.7. Elemental analysis calc (%) for

$[Cr(phen)_3](CF_3SO_3)_3 \cdot 1.2H_2O$: C 43.13, H 2.51, N 7.92; found: C 44.05, H 2.39, N 7.85. Elemental analysis calc (%) for ($[Cr(phen)_3](PF_6)_3$): C 42.08, H 2.35, N 8.18; found: C 42.25, H 2.38, N 8.10.

Preparation of $[Cr(phen)_2(phenBr)](PF_6)_3$ (3). $[Cr(phen)_2(CF_3SO_3)_2](CF_3SO_3)$ (51 mg, 0.06 mmol), 5-bromo-1,10-phenanthroline (38 mg, 0.15 mmol), and anhydrous distilled dichloromethane (7 mL) were introduced into a Schlenk tube. The reaction mixture was heated at 45°C for 3 h. The formed yellow solid was filtered on a ptfe membrane, washed with CH_2Cl_2 and dried with Et_2O to give pure $[Cr(phen)_2(phenBr)](CF_3SO_3)_3$ (44 mg, 0.04 mmol, yield 66%). Metathesis resulted from the dissolution of $[Cr(phen)_2(phenBr)](CF_3SO_3)_3$ in a minimum amount of MeOH, followed by the addition of a saturated solution of $TBAPF_6$ in MeOH. The precipitate of $[Cr(phen)_2(phenBr)](PF_6)_3$ was filtered and dried. Slow diffusion of Et_2O into a solution of $[Cr(phen)_2(phenBr)](PF_6)_3$ in acetonitrile provided single crystals suitable for XRD. ESI-MS *m/z*: $[[Cr(phen)_2(phenBr)](CF_3SO_3)_2]^+$ 970.6. Elemental analysis calc (%) for $[Cr(phen)_2(phenBr)](CF_3SO_3)_3 \cdot 2H_2O$: C 40.57, H 2.36, N 7.28; found: C 40.48, H 2.51, N 7.14.

General preparation of $[Cr(phen)_2(N\text{-}N')](CF_3SO_3)_3$ complexes. $[Cr(phen)_2Cl_2]Cl$ (1 eq) and trifluoromethanesulfonic acid (1 mL per 120 mg of $[Cr(phen)_2Cl_2]Cl$) were introduced into a Schlenk tube under argon and heated at 100°C for two hours with argon bubbling. The solution was cooled on ice and vigorously stirred. Anhydrous distilled diethyl ether (10 mL per 200-300 mg of $[Cr(phen)_2Cl_2]Cl$) was added, thus leading to the formation of a pink precipitate. The solid was filtered under argon and washed twice with anhydrous diethyl ether, rapidly dissolved in distillated CH_2Cl_2 (10 mL) and transferred under argon into a Schlenck tube containing the N-N' ligand, pyridine or 2,6-lutidine, and distillated CH_2Cl_2 (10 mL). The resulting mixture was stirred at 45 °C during 2 to 16h until formation of a large amount of precipitate. The solid was collected by filtration on a ptfe

membrane, washed with CH_2Cl_2, and dried with Et_2O to give $[Cr(phen)_2(N\text{-}N')](CF_3SO_3)_3$ complexes as a microcrystalline solids.

Preparation of $[Cr(phen)_2(phenAlkyn)](BF_4)_3$ (6). This complex was synthetized according to the general synthetic method described for $[Cr(phen)_2(N\text{-}N')](CF_3SO_3)_3$ complexes.

$[Cr(phen)_2Cl_2]Cl$ (200 mg, 0.387 mmol, 1 eq), trifluoromethanesulfonic acid (2 mL), 5-ethynyl-1,10-phenanthroline (79 mg, 0.387 mmol, 1 eq), pyridine (62 µL, 0.774 mmol, 2 eq). Reaction time: 2h.

This method afforded pure $[Cr(phen)_2(phenAlkyn)](CF_3SO_3)_3$ (300 mg, 73 %). Metathesis resulted from the dissolution of $[Cr(phen)_2(phenBr)](CF_3SO_3)_3$ in a minimum amount of MeOH, followed by the addition of a saturated solution of $TBABF_4$ in MeOH. The precipitate of $[Cr(phen)_2(phenAlkyn)](BF_4)_3$ was filtered and dried. Slow diffusion of Et_2O into a solution of $[Cr(phen)_2(phenAlkyn)](BF_4)_3$ in acetonitrile provided single crystals suitable for XRD. ESI-MS *m/z*: $[[Cr(phen)_2(phenAlkyn)](CF_3SO_3)_2]^+$ 914.5. Elemental analysis calc (%) for $[Cr(phen)_2(phenAlkyn)](CF_3SO_3)_3 \cdot 2.5\ H_2O$: C 44.41, H 2.64, N 7.58; found: C 44.37, H 2.53, N 7.63. Elemental analysis calc (%) for $[Cr(phen)_2(phenAlkyn)](BF_4)_3 \cdot 1.2\ H_2O$: C 50.91, H 2.96, N 9.35; found: C 50.91, H 3.00, N 9.23.

Preparation of $[Cr(phen)_2(phenNO_2)](CF_3SO_3)_3$ (7). The complex was synthetized according to the general synthetic method described for $[Cr(phen)_2(N\text{-}N')](CF_3SO_3)_3$ complexes.

$[Cr(phen)_2Cl_2]Cl$ (200 mg, 0.387 mmol, 1 eq), trifluoromethanesulfonic acid (2 mL), 5-nitro-1,10-phenanthroline (176 mg, 0.772 mmol, 2 eq), 2,6-lutidine (45 µL, 0.386 mmol, 1 eq). Reaction time: 16h. The resulting yellow powder was suspended in CH_2Cl_2, stirred thoroughly for 24h, filtered on a ptfe membrane, washed with CH_2Cl_2 and dried with Et_2O to give pure $[Cr(phen)_2(phenNO_2)](CF_3SO_3)_3$ (186 mg, yield 44 %). Slow diffusion of Et_2O in a solution of $[Cr(phen)_2(phenNO_2)](CF_3SO_3)_3$ in methanol provided single crystals suitable for XRD. ESI-MS *m/z*: $[[Cr(phen)_2(phenNO_2)](CF_3SO_3)_2]^+$

935.5. Elemental analysis calc (%) for $[Cr(phen)_2(phenNO_2)](CF_3SO_3)_3 \cdot 2.5\ H_2O$: C 41.46, H 2.50, N 8.68; found: C 41.41, H 2.38, N 8.63.

Preparation of $[Cr(phen)_2(phenNH_2)](CF_3SO_3)_3$ (8). The complex was synthetized according to the general synthetic method described for $[Cr(phen)_2(N\text{-}N')](CF_3SO_3)_3$ complexes.

$[Cr(phen)_2Cl_2]Cl$ (200 mg, 0.387 mmol, 1 eq), trifluoromethanesulfonic acid (2 mL), 5-amino-1,10-phenanthroline (90 mg, 0.463 mmol, 1.2 eq), pyridine (50 µL, 0.521 mmol, 1.35 eq). Reaction time: 16h. The resulting brown powder was thoroughly washed with THF, filtered on a ptfe membrane, washed with CH_2Cl_2 and dried with Et_2O to give pure $[Cr(phen)_2(phenNH_2)](CF_3SO_3)_3$ (260 mg, yield 64 %). Slow diffusion of Et_2O into a solution of $[Cr(phen)_2(phenNH_2)](CF_3SO_3)_3$ in acetonitrile provided single crystals suitable for XRD. ESI-MS *m/z*: $[[Cr(phen)_2(phenNH_2)](CF_3SO_3)_2]^+$ 905.5. Elemental analysis calc (%) for $[Cr(phen)_2(phenNH_2)](CF_3SO_3)_3 \cdot 1.5\ H_2O$: C 43.30, H 2.61, N 9.06; found: C 43.40, H 2.70, N 8.96.

Preparation of $[Cr(phen)_2(bipy)](BF_4)_3$ (9). The complex was synthetized according to the general synthetic method described for $[Cr(phen)_2(N\text{-}N')](CF_3SO_3)_3$ complexes.

$[Cr(phen)_2Cl_2]Cl$ (300 mg, 0.578 mmol, 1 eq), trifluoromethanesulfonic acid (2.2 mL), bipyridine (181 mg, 1.16 mmol, 2 eq), pyridine (93 µL, 1.16 mmol, 2 eq). Reaction time: 2h. This method afforded pure $[Cr(phen)_2(bipy)](CF_3SO_3)_3$ (444 mg, yield 76 %). Metathesis resulted from the dissolution of $[Cr(phen)_2(phenBr)](CF_3SO_3)_3$ in a minimum amount of MeOH, followed by the addition of a saturated solution of $TBABF_4$ in MeOH. The precipitate of $[Cr(phen)_2(bipy)](BF_4)_3$ was filtered and dried. Slow diffusion of Et_2O into a solution of $[Cr(phen)_2(bipy)](BF_4)_3$ in acetonitrile provided single crystals suitable for XRD. ESI-MS *m/z*: $[[Cr(phen)_2(bipy)](CF_3SO_3)_2]^+$ 866.5. Elemental analysis calc (%) for $[Cr(phen)_2(bipy)](CF_3SO_3)_3 \cdot 1.3CH_2Cl_2$: C 40.85, H 2.38, N 7.46; found: C 40.70, H 2.39, N 7.61.

Elemental analysis calc (%) for $[Cr(phen)_2(bipy)](BF_4)_3 \cdot 1.3\ H_2O$: C 47.91, H 3.15, N 9.86; found: C 47.87, H 3.16, N 9.83.

Preparation of $[Cr(phen)_2(dpma)](CF_3SO_3)_3$ (10). The complex was synthetized according to the general synthetic method described for $[Cr(phen)_2(N\text{-}N')](CF_3SO_3)_3$ complexes.

$[Cr(phen)_2Cl_2]Cl$ (200 mg, 0.387 mmol, 1 eq), trifluoromethanesulfonic acid (2 mL), di(pyrid-2-yl)(methyl)amine) (143 mg, 0.772 mmol, 2 eq), 2,6-lutidine (90 µL, 0.772 mmol, 2 eq). Reaction time: 2h. This method afforded pure $[Cr(phen)_2(dpma)](CF_3SO_3)_3$ (241 mg, yield 60 %). Slow diffusion of Et_2O into a solution of $[Cr(phen)_2(dpma)](CF_3SO_3)_3$ in methanol provided single crystals suitable for XRD. ESI-MS *m/z*: $[[Cr(phen)_2(dpma)](CF_3SO_3)_2]^+$ 895.3. Elemental analysis calc (%) for $[Cr(phen)_2(dpma)](CF_3SO_3)_3 \cdot 0.35\ H_2O$: C 43.42, H 2.66, N 9.33; found: C 43.31, H 2.55, N 9.25.

Photophysical measurements. Absorption spectra in solution were recorded using a Lambda 1050 Perkin Elmer spectrometer (quartz cell path length 1 cm or 1 mm, 300-800 nm domain). Absorption spectra in the solid state were recorded on a Lambda 900 Perkin Elmer spectrometer equipped with an integration sphere (background recorded on MgO). Emission spectra (excitation at 355 nm) and excitation spectra were recorded for frozen solution samples (acetonitrile/propionitrile 6/4 at $C \approx 5\times10^{-3}$ mol/L), for powder samples at 10 K or for freeze pump thaw degassed acetonitrile solution ($C \approx 10^{-4}$ mol/L) at 293 K, with a Fluorolog (Horiba Jobin-Yvon), equipped with iHR320, a Xenon lamp 450 Watt Illuminator (FL-1039A/40A) and a water-cooled photo multiplier tube (PMT Hamamatsu R2658 or R928). The spectra were corrected for the spectral response of the system. For time-resolved experiments, the decay curves were collected on solution samples (acetonitrile/propionitrile 6/4 at $C \approx 5\times10^{-3}$ mol/L) within the 10 K to 300 K range, with a photomultiplier (Hamamatsu R2658 or R928) and a digital oscilloscope (Tektronix MDO4104C). Pulsed excitation at 355 nm was obtained with the third harmonic of a pulsed Nd:YAG laser (Quantel Qsmart850). Low temperatures were achieved with

a closed cycle cryosystem (Janis, CCS-900/204N) with the sample sitting in exchange gas (helium) for efficient cooling. Microcrystalline samples or acetonitrile/propionitrile (6/4) solutions ($C \approx 5\times10^{-3}$ mol/L) were mounted in glass capillary (1.2 mm interior diameter, glass cutoff at 320 nm) and stuck on copper plates with Agar scientific silver paint (G3691). The copper plates were attached to the sample holder with silver paint as well. The oxygen free decay curve measurements were done at 293 K on acetonitrile solutions of the complex ($C \approx 10^{-4}$ mol/L). The complexes in quartz tube were dissolved in acetonitrile then degassed by freeze pump thaw, and filled with argon.

X-ray crystallography

All data were collected on a Rigaku Supernova diffractometer equipped with a CCD ATLAS detector using Mo or Cu Kα radiation. The crystals were mounted on Mitegen cryoloops and held at 180 K in the cold stream of a cryostream (oxford cryosystems). Structures were solved using the dual-space algorithm implemented in SHELXT,[BD81] or using direct methods within the SIR2004 program.[BD82] They were refined using the *full-matrix least-squares method* on F^2 in the SHELXL program,[BD83] within the framework of the Olex2 Software.[BD84] CCDC 1865017-1865025 contain the supplementary crystallographic data for this paper. The data can be obtained free of charge from The Cambridge Crystallographic Data Centre via www.ccdc.cam.ac.uk/structures.

ASSOCIATED CONTENT

The Supporting Information is available free of charge and contains crystallographic data, absorption, excitation, and emission spectrum, list of transition band, list of lifetimes, and decay curves.

AUTHOR INFORMATION

Corresponding Author

*Benjamin Doistau, E-mail: benjamin.doistau@unige.ch

*Claude Piguet, E-mail: claude.piguet@unige.ch

Present Addresses

† G.C.: Centre de Biophysique Moléculaire (CBM) ; UPR CNRS 4301, Rue Charles Sadron, F-45071 Orléans 2, France

Author Contributions

The manuscript was written through contributions of all authors. All authors have given approval to the final version of the manuscript.

Funding Sources

Financial support from the Swiss National Science Foundation is gratefully acknowledged.

Notes

The authors declare no competing financial interest.

ACKNOWLEDGMENT

K. L. Buchwalder is acknowledged for performing elemental analysis.

REFERENCES

BD1 Büldt, L. A.; Wenger, O. S. Chromium Complexes for Luminescence, Solar Cells, Photoredox Catalysis, Upconversion, and Phototriggered NO Release. *Chem. Sci.* **2017**, *8*, 7359-7367.

BD2 Büldt, L. A.; Wenger, O. S. Luminescent Complexes Made from Chelating Isocyanide Ligands and Earth-abundant Metals. *Dalton Trans.* **2017**, *46*, 15175-15175.

BD3 Kahn, O.; Briat, B. Exchange Interaction in Polynuclear Complexes. Part 1.-Principles, Model and Application to the Binuclear Complexes of Chromium(III). *J. Chem. Soc., Faraday Trans. 2* **1976**, *72*, 268-281.

BD4 Carlin, R. L.; Burriel, R. Magnetic Susceptibility of $Cs_2CrCl_5.4H_2O$: Interplay of Exchange and Crystal-field Effects. *Phys. Rev. B* **1983**, *27*, 3012-3017.

BD5 Timco, G. A.; McInnes, E. J. L.; Winpenny, R. E. P. Physical studies of Heterometallic Rings: An Ideal System for Studying Magnetically-coupled Systems. *Chem. Soc. Rev.* **2013**, *42*, 1796-1806.

BD6 Morsing, T. J.; Sauer, S. P. A.; Weihe, H.; Bendix, J.; Døssing, A. Magnetic Interactions in Oxide-bridged Dichromium(III) Complexes. Computational Determination of the Importance of Non-bridging Ligands. *Inorg. Chim. Acta* **2013**, *396*, 72-77.

BD7 Collison, D.; Murrie, M.; Oganesyan, V. S.; Piligkos, S.; Poolton, N. R. J.; Rajaraman, G.; Smith, G. M.; Thomson, A. J.; Timko, G. A.; Wernsdorfer, W.; Winpenny, R. E. P.; McInnes, E. J. L. Magnetic and Optical Studies on an S = 6 Ground-State Cluster $[Cr_{12}O_9(OH)_3(O_2CCMe_3)_{15}]$: Determination of, and the Relationship Between, Single-Ion and Cluster Spin Hamiltonian Parameters. *Inorg. Chem.* **2003**, *42*, 5293-5303.

BD8 Novosel, N.; Žilić, D.; Pajić, D.; Jurić, M.; Perić, B.; Zadro, K.; Rakvin, B.; Planinić, P. EPR and Magnetization Studies on Single Crystals of a Heterometallic (Cu(II) and Cr(III)) Complex: Zero-field Splitting Determination. *Solid State Sci.* **2008**, *10*, 1387-1394.

BD9 Alonso, P. J.; Arauzo, A. B.; Garcia-Monforte, M. A.; Garcia-Rubio, I.; Martin, A.; Menjon, B.; Rillo, C. Synthesis, Characterisation and Magnetic Properties of Octahedral Chromium(III) Compounds with Six C-donor Ligands. *Dalton Trans.* **2011**, *40*, 853-861.

BD10 Padhi, S. K.; Saha, D.; Sahu, R.; Subramanian, J.; Manivannan, V. Synthesis, Structure, Optical and Magnetic Properties of $[CrL(X)_3]$, {L = 4′-(2-pyridyl)-2,2′:6′,2″-terpyridine; X = Cl−, N_3−, NCS−}. *Polyhedron* **2008**, *27*, 1714-1720.

BD11 Scarborough, C. C.; Lancaster, K. M.; DeBeer, S.; Weyhermüller, T.; Sproules, S.; Wieghardt, K. Experimental Fingerprints for Redox-Active Terpyridine in $[Cr(tpy)_2](PF_6)_n$ (n = 3–0), and the Remarkable Electronic Structure of $[Cr(tpy)_2]^{1-}$. *Inorg. Chem.* **2012**, *51*, 3718-3732.

BD12 Mallah, T.; Thiébaut, S.; Verdaguer, M.; Veillet, P. High-T_C Molecular-Based Magnets: Ferrimagnetic Mixed-Valence Chromium(III)-Chromium(II) Cyanides with T_C at 240 and 190 Kelvin. *Science* **1993**, *262*, 1554.

BD13 Verdaguer, M.; Bleuzen, A.; Marvaud, V.; Vaissermann, J.; Seuleiman, M.; Desplanches, C.; Scuiller, A.; Train, C.; Garde, R.; Gelly, G.; Lomenech, C.; Rosenman, I.; Veillet, P.; Cartier, C.; Villain, F. Molecules to Build Solids: High T_C Molecule-based Magnets by Design and Recent Revival of Cyano Complexes Chemistry. *Coord. Chem. Rev.* **1999**, *190–192*, 1023-1047.

BD14 McInnes, E. J. L.; Piligkos, S.; Timco, G. A.; Winpenny, R. E. P. Studies of Chromium Cages and Wheels. *Coord. Chem. Rev.* **2005**, *249*, 2577-2590.

BD15 Marinescu, G.; Andruh, M.; Lloret, F.; Julve, M. Bis(oxalato)chromium(III) complexes: Versatile Tectons in Designing Heterometallic Coordination Compounds. *Coord. Chem. Rev.* **2011**, *255*, 161-185.

BD16 Regula, S.; Silvio, D.; Helen, S. E.; Claire, W.; Dima, Y.; K., H. J. A.; C., C. S.; Andreas, H. A Thermal Spin Transition in $[Co(bpy)_3][LiCr(ox)_3]$ (ox=$C_2O_4^{2-}$; bpy=2,2′-bipyridine). *Chem. Eur. J.* **2000**, *6*, 361-368.

BD17 Kou, H.-Z.; Zhou, B. C.; Gao, S.; Wang, R.-J. A 2D Cyano- and Oxamidato-Bridged Heterotrimetallic Cr(III)-Cu(II)-Gd(III) Complex. *Angew. Chem. Int. Ed.* **2003**, *42*, 3288-3291.

BD18 Kandasamy, B.; Ramar, G.; Zhou, L.; Han, S.-T.; Venkatesh, S.; Cheng, S.-C.; Xu, Z.; Ko, C.-C.; Roy, V. A. L. Polypyridyl Chromium(III) Complexes for Non-volatile Memory Application: Impact of the Coordination Sphere on Memory Device Performance. *J. Mater. Chem. C* **2018**, *6*, 1445-1450.

BD19 McDaniel, A. M.; Tseng, H.-W.; Damrauer, N. H.; Shores, M. P. Synthesis and Solution Phase Characterization of Strongly Photooxidizing Heteroleptic Cr(III) Tris-Dipyridyl Complexes. *Inorg. Chem.* **2010**, *49*, 7981-7991.

BD20 Stevenson, S. M.; Shores, M. P.; Ferreira, E. M. Photooxidizing Chromium Catalysts for Promoting Radical Cation Cycloadditions. *Angew. Chem. Int. Ed.* **2015**, *54*, 6506-6510.

BD21 Higgins, R. F.; Fatur, S. M.; Shepard, S. G.; Stevenson, S. M.; Boston, D. J.; Ferreira, E. M.; Damrauer, N. H.; Rappé, A. K.; Shores, M. P. Uncovering the Roles of Oxygen in Cr(III) Photoredox Catalysis. *J. Am. Chem. Soc.* **2016**, *138*, 5451-5464.

BD22 Stevenson, S. M.; Higgins, R. F.; Shores, M. P.; Ferreira, E. M. Chromium Photocatalysis: Accessing Structural Complements to Diels-Alder Adducts with Electron-deficient Dienophiles. *Chem. Sci.* **2017**, *8*, 654-660.

BD23 Maeda, K.; Teramura, K.; Lu, D.; Takata, T.; Saito, N.; Inoue, Y.; Domen, K. Photocatalyst Releasing Hydrogen from Water. *Nature* **2006**, *440*, 295.

BD24 Kirk, A. D. Chromium(III) Photochemistry and Photophysics. *Coord. Chem. Rev.* **1981**, *39*, 225-263.

BD25 Jamieson, M. A.; Serpone, N.; Hoffman, M. Z. Advances in the Photochemistry and Photophysics of Chromium(III) Polypyridyl Complexes in Fluid Media. *Coord. Chem. Rev.* **1981**, *39*, 121-179.

BD26 Forster, L. S. The Photophysics of Chromium(III) Complexes. *Chem. Rev.* **1990**, *90*, 331-353.

BD27 Kirk, A. D. Photochemistry and Photophysics of Chromium(III) Complexes. *Chem. Rev.* **1999**, *99*, 1607-1640.

BD28 Forster, L. S. Thermal Relaxation in Excited Electronic States of d^3 and d^6 Metal Complexes. *Coord. Chem. Rev.* **2002**, *227*, 59-92.

BD29 Ryu, C. K.; Endicott, J. F. Synthesis, Spectroscopy, and Photophysical Behavior of Mixed-ligand Mono- and Bis(polypyridyl)chromium(III) Complexes. Examples of Efficient, Thermally Activated Excited-state Relaxation without Back Intersystem Crossing. *Inorg. Chem.* **1988**, *27*, 2203-2214.

BD30 Zare, D.; Doistau, B.; Nozary, H.; Besnard, C.; Guenee, L.; Suffren, Y.; Pele, A.-L.; Hauser, A.; Piguet, C. Cr(III) as an Alternative to Ru(II) in Metallo-Supramolecular Chemistry. *Dalton Trans.* **2017**, *46*, 8992-9009.

BD31 Otto, S.; Dorn, M.; Förster, C.; Bauer, M.; Seitz, M.; Heinze, K. Understanding and Exploiting Long-lived Near-infrared Emission of a Molecular Ruby. *Coord. Chem. Rev.* **2018**, *359*, 102-111.

BD32 Aboshyan-Sorgho, L.; Besnard, C.; Pattison, P.; Kittilstved, K. R.; Aebischer, A.; Bünzli, J.-C. G.; Hauser, A.; Piguet, C. Near-Infrared→Visible Light Upconversion in a Molecular Trinuclear d–f–d Complex. *Angew. Chem. Int. Ed.* **2011**, *50*, 4108-4112.

BD33 Suffren, Y.; Zare, D.; Eliseeva, S. V.; Guénée, L.; Nozary, H.; Lathion, T.; Aboshyan-Sorgho, L.; Petoud, S.; Hauser, A.; Piguet, C. Near-Infrared to Visible Light-Upconversion in Molecules: From Dream to Reality. *J. Phys. Chem. C* **2013**, *117*, 26957-26963.

BD34 Zare, D.; Suffren, Y.; Guenee, L.; Eliseeva, S. V.; Nozary, H.; Aboshyan-Sorgho, L.; Petoud, S.; Hauser, A.; Piguet, C. Smaller than a Nanoparticle with the Design of Discrete Polynuclear Molecular Complexes Displaying Near-infrared to Visible Upconversion. *Dalton Trans.* **2015**, *44*, 2529-2540.

BD35 Suffren, Y.; Golesorkhi, B.; Zare, D.; Guénée, L.; Nozary, H.; Eliseeva, S. V.; Petoud, S.; Hauser, A.; Piguet, C. Taming Lanthanide-Centered Upconversion at the Molecular Level. *Inorg. Chem.* **2016**, *55*, 9964-9972.

BD39 J., C. L.; Niko, H. Lanthanide Complexes and Quantum Dots: A Bright Wedding for Resonance Energy Transfer. *Eur. J. Inorg. Chem.* **2008**, *2008*, 3241-3251.

BD40 Tanner, P. A.; Zhou, L.; Duan, C.; Wong, K.-L. Misconceptions in Electronic Energy Transfer: Bridging the Gap Between Chemistry and Physics. *Chem. Soc. Rev.* **2018**, *47*, 5234-5265.

BD41 Serpone, N.; Jamieson, M. A.; Henry, M. S.; Hoffman, M. Z.; Bolletta, F.; Maestri, M. Excited-state Behavior of Polypyridyl Complexes of Chromium(III). *J. Am. Chem. Soc.* **1979**, *101*, 2907-2916.

BD42 Kirk, A. D.; Porter, G. B. Luminescence of Chromium(III) Complexes. *J. Phys. Chem.* **1980**, *84*, 887-891.

BD43 Endicott, J. F.; Lessard, R. B.; Lynch, D.; Perkovic, M. W.; Ryu, C. K. Stereochemical and Electronic Contributions to ^{2}E Chromium(III) Excited Sstate Relaxation Behavior at 77K. *Coord. Chem. Rev.* **1990**, *97*, 65-79.

BD44 Barker, K. D.; Barnett, K. A.; Connell, S. M.; Glaeser, J. W.; Wallace, A. J.; Wildsmith, J.; Herbert, B. J.; Wheeler, J. F.; Kane-Maguire, N. A. P. Synthesis and Characterization of Heteroleptic $[Cr(diimine)_3]^{3+}$ Complexes. *Inorg. Chim. Acta* **2001**, *316*, 41-49.

BD45 Donnay, E. G.; Schaeper, J. P.; Brooksbank, R. D.; Fox, J. L.; Potts, R. G.; Davidson, R. M.; Wheeler, J. F.; Kane-Maguire, N. A. P. Synthesis and Characterization of Tris(heteroleptic) Diimine Complexes of Chromium(III). *Inorg. Chim. Acta* **2007**, *360*, 3272-3280.

BD46 Isaacs, M.; Sykes, A. G.; Ronco, S. Synthesis, Characterization and Photophysical Properties of Mixed Ligand Tris(polypyridyl)chromium(III) Complexes, $[Cr(phen)_2L]^{3+}$. *Inorg. Chim. Acta* **2006**, *359*, 3847-3854.

BD47 Barbour, J. C.; Kim, A. J. I.; deVries, E.; Shaner, S. E.; Lovaasen, B. M. Chromium(III) Bis-Arylterpyridyl Complexes with Enhanced Visible Absorption via Incorporation of Intraligand Charge-Transfer Transitions. *Inorg. Chem.* **2017**, *56*, 8212-8222.

BD48 Cantuel, M.; Bernardinelli, G.; Imbert, D.; Bunzli, J.-C. G.; Hopfgartner, G.; Piguet, C. A Kinetically Inert and Optically Active Cr(III) Partner in Thermodynamically Self-assembled Heterodimetallic Non-covalent d-f Podates. *J. Chem. Soc., Dalton Trans.* **2002**, 1929-1940.

BD49 Cantuel, M.; Bernardinelli, G.; Muller, G.; Riehl, J. P.; Piguet, C. The First Enantiomerically Pure Helical Noncovalent Tripod for Assembling Nine-Coordinate Lanthanide(III) Podates. *Inorg. Chem.* **2004**, *43*, 1840-1849.

BD50 Cantuel, M.; Gumy, F.; Bunzli, J.-C. G.; Piguet, C. Encapsulation of Labile Trivalent Lanthanides into a Homobimetallic Chromium(III)-containing Triple-stranded Helicate. Synthesis, Characterization, and Divergent Intramolecular Energy Transfers. *Dalton Trans.* **2006**, 2647-2660.

BD51 Aboshyan-Sorgho, L.; Cantuel, M.; Petoud, S.; Hauser, A.; Piguet, C. Optical Sensitization and Upconversion in Discrete Polynuclear Chromium–lanthanide Complexes. *Coord. Chem. Rev.* **2012**, *256*, 1644-1663.

BD52 Imbert, D.; Cantuel, M.; Bünzli, J.-C. G.; Bernardinelli, G.; Piguet, C. Extending Lifetimes of Lanthanide-Based Near-Infrared Emitters (Nd, Yb) in the Millisecond Range through Cr(III) Sensitization in Discrete Bimetallic Edifices. *J. Am. Chem. Soc.* **2003**, *125*, 15698-15699.

BD61 Vasudevan, S.; Smith, J. A.; Wojdyla, M.; McCabe, T.; Fletcher, N. C.; Quinn, S. J.; Kelly, J. M. Substituted Dipyridophenazine Complexes of Cr(III): Synthesis, Enantiomeric Resolution and Binding Interactions with Calf Thymus DNA. *Dalton Trans.* **2010**, *39*, 3990-3998.

BD62 The crystal structure of $[Cr(phen)_2Cl_2]Cl$ was previously reported with a different space group and unit cell. Gao, X. cis-Dichloridobis(1,10-phenanthroline)chromium(III) Chloride. *Acta Crystallographica Section E: Structure Reports Online* **2011**, *67*, m139-m139.

BD63 The crystal structure of $[Cr(phen)_3](ClO_4)$ was reported by Luck, R. L.; Gawryszewska, P.; Riehl, J. P. Tris(1,10-phenanthroline-N,N')chromium(III) Triperchlorate Hydrate. *Acta Crystallographica Section C* **2000**, *56*, e238-e239.

BD88 Scarborough, C. C.; Sproules, S.; Doonan, C. J.; Hagen, K. S.; Weyhermüller, T.; Wieghardt, K. Scrutinizing Low-Spin Cr(II) Complexes. *Inorg. Chem.* **2012**, *51*, 6969-6982.

BD64 Pearson, R. G.; Munson, R. A.; Basolo, F. Mechanism of Substituion Reactions of Complex Ions. XV: Acid and Base Hydrolysis of Cis- and Trans-dichloro-bis-(ethylene-diamine)-chromium(III) Ion. *J. Am. Chem. Soc.* **1958**, *80*, 504-504.

BD54 Wang, C.; Otto, S.; Dorn, M.; Kreidt, E.; Lebon, J.; Sršan, L.; Di Martino-Fumo, P.; Gerhards, M.; Resch-Genger, U.; Seitz, M.; Heinze, K. Deuterated Molecular Ruby with Record Luminescence Quantum Yield. *Angew. Chem. Int. Ed.* **2017**, *57*, 1112-1116.

BD58 Breivogel, A.; Meister, M.; Förster, C.; Laquai, F.; Heinze, K. Excited State Tuning of Bis(tridentate) Ruthenium(II) Polypyridine Chromophores by Push–Pull Effects and Bite Angle Optimization: A Comprehensive Experimental and Theoretical Study. *Chem. Eur. J.* **2013**, *19*, 13745-13760.

BD36 Otto, S.; Grabolle, M.; Förster, C.; Kreitner, C.; Resch-Genger, U.; Heinze, K. $[Cr(ddpd)_2]^{3+}$: A Molecular, Water-Soluble, Highly NIR-Emissive Ruby Analogue. *Angew. Chem. Int. Ed.* **2015**, *54*, 11572-11576.

BD37 Jorgensen, C. K. Spectroscopy of Transition-group Complexes. *Adv. Chem. Phys.* **1963**, *5*, 33-146.

BD38 Lever, A. B. P. *Inorganic Electronic Spectroscopy*; Elsevier ed., 1984, p. 126.

BD53 Kane-Maguire, N. A. P. Photochemistry and Photophysics of Coordination Compounds: Chromium. *Top. Curr. Chem.* **2007**, *280*, 37-67.

BD55 Perkovic, M. W.; Heeg, M. J.; Endicott, J. F. Stereochemical Perturbations of the Relaxation Behavior of (^{2}E)Chromium(III). Ground-state X-ray Crystal Structure, Photophysics, and Molecular Mechanics Simulations of the Quasi-cage Complex [4,4',4"-Ethylidynetris(3-azabutan-1-amine)]chromium Tribromide. *Inorg. Chem.* **1991**, *30*, 3140-3147.

BD56 Hauser, A.; Maeder, M.; Robinson, W. T.; Murugesan, R.; Ferguson, J. Electronic and Molecular Structure of Tris(2,2'-bipyridine)chromium(3+). *Inorg. Chem.* **1987**, *26*, 1331-1338.

BD57 Lee, K.-W.; Hoggard, P. E. The Molecular Structure of Bipyridinium tris(bipyridine)chromium(III) Perchlorate. *Polyhedron* **1989**, *8*, 1557-1560.

BD85 Ohno, T.; Kato, S.; Kaizaki, S.; Hanazaki, I. Singlet-triplet transitions of aromatic compounds coordinating to a paramagnetic chromium(III) ion. *Inorg. Chem.* **1986**, *25*, 3853-3858.

BD87 König, E.; Herzog, S. Electronic spectra of tris(2,2′-bipyridyl) complexes—I: The chromium series [Cr(bipy)3]z, z = +3, +2, +1, 0. *Journal of Inorganic and Nuclear Chemistry* **1970**, *32*, 585-599.

BD65 Otto, S.; Scholz, N.; Behnke, T.; Resch-Genger, U.; Heinze, K. Thermo-Chromium: A Contactless Optical Molecular Thermometer. *Chem. Eur. J.* **2017**, *23*, 12131-12135.

BD66 Morse, P. M. Diatomic Molecules According to the Wave Mechanics. II. Vibrational Levels. *Phys. Rev.* **1929**, *34*, 57-64.

BD67 Hansch, C.; Leo, A.; Taft, R. W. A Survey of Hammett Substituent Constants and Resonance and Field Parameters. *Chem. Rev.* **1991**, *91*, 165-195.

BD75 Kuehn, K.; Wasgestian, F.; Kupka, H. The Role of Hydrogen Vibrations in the Radiationless Deactivation of Chromium(III)-Alkylamine Complexes in their Lowest Doublet State. *J. Phys. Chem.* **1981**, *85*, 665-670.

BD76 N. Brown, K.; J. Geue, R.; M. Sargeson, A.; Moran, G.; F. Ralph, S.; Riesen, H. A Long-Lived ^{2}E State for a Cr(III)N_6 Amine cChromophore at 298 K: [Cr(fac-Me_5-D_{3h}tricosaneN_6)]Cl_3. *Chem. Commun.* **1998**, 2291-2292.

BD86 Otto, S.; Förster, C.; Wang, C.; Resch-Genger, U.; Heinze, K. A Strongly Luminescent Chromium(III) Complex Acid. *Chem. Eur. J.* **2018**, *24*, 12555-12563.

BD68 Einstein, A. Zur Quantentheorie der Strahlung. *Phys. Z.* **1917**, *18*, 121–128.

BD69 Strickler, S J.; Berg, R. A. Relationship Between Absorption Intensity and Fluorescence Lifetime of Molecules. *J. Chem. Phys.* **1962**, *37*, 814–822.

BD70 Berks, J. B.; Dyson, D. J. The Relations Between the Fluorescence and Absorption Properties of Organic Molecules. *Proc. R. London Soc. Ser. A* **1963**, *275*, 135–148.

BD71 Perkovic, M. W.; Endicott, J. F. Stereochemical Tuning of Chromium(III) Photophysics with *N,N′,N″*-Tris(alkylamine)-1,4,7-tTriazacyclononane Complexes. *J. Phys. Chem.* **1990**, *94*, 1217-1219.

BD72 Fucaloro, A. F.; Forster, L. S.; Rund, J. V.; Lin, S. H. ^{2}E Relaxation in Mixed-Ligand Cr$(NH_3)_{6-n}X_n$ Complexes. *J. Phys. Chem.* **1983**, *87*, 1796-1799.

BD73 Rojas, G. E.; Magde, D. Temperature dependence of the doublet lifetime in chromium(III) compounds. *Inorg. Chem.* **1987**, *26*, 2334-2337.

BD74 Castelli, F.; Forster, L. S. Nonexponential Luminescence Decay in Hexaureachromium(III). *J. Am. Chem. Soc.* **1975**, *97*, 6306-6309.

BD77 Ji, S.; Guo, H.; Yuan, X.; Li, X.; Ding, H.; Gao, P.; Zhao, C.; Wu, W.; Wu, W.; Zhao, J. A Highly Selective OFF-ON Red-Emitting Phosphorescent Thiol Probe with Large Stokes Shift and Long Luminescent Lifetime. *Org. Lett.* **2010**, *12*, 2876-2879.

BD78 Wu, S. H.; Shao, J. Y.; Dai, X.; Cui, X.; Su, H.; Zhong, Y. W. Synthesis and Characterization of Tris(bidentate) Ruthenium Complexes of Di(pyrid-2-yl)(methyl)amine. *Eur. J. Inorg. Chem.* **2017**, *2017*, 3064-3071.

BD79 Hissler, M.; Connick, W. B.; Geiger, D. K.; McGarrah, J. E.; Lipa, D.; Lachicotte, R. J.; Eisenberg, R. Platinum Diimine Bis(acetylide) Complexes: Synthesis, Characterization, and Luminescence Properties. *Inorg. Chem.* **2000**, *39*, 447-457.

BD80 Burstall, F. H.; Nyholm, R. S. 681. Studies in Co-ordination Chemistry. Part XIII. Magnetic Moments and Bond Types of Transition-Metal Complexes. *J. Chem. Soc.* **1952**, 3570-3579.

BD81 Sheldrick, G. SHELXT - Integrated Space-group and Crystal-structure Determination. *Acta Crystallogr., Sect. A* **2015**, *71*, 3-8.

BD82 Burla, M. C.; Caliandro, R.; Camalli, M.; Carrozzini, B.; Cascarano, G. L.; De Caro, L.; Giacovazzo, C.; Polidori, G.; Spagna, R. SIR2004: an improved tool for crystal structure determination and refinement. *J. Appl. Crystallogr.* **2005**, *38*, 381-388.

BD83 Sheldrick G. M. Crystal structure refinement with SHELXL. *Acta Cryst C*. **2015**, *71*, 3–8.

BD84 Dolomanov, O. V.; Bourhis, L. J.; Gildea, R. J.; Howard, J. A. K.; Puschmann, H. OLEX2: a complete structure solution, refinement and analysis program. *J. Appl. Crystallogr.* **2009**, *42*, 339-341.

SYNOPSIS

A family of heteroleptic $[Cr(phen)_2(N\text{-}N')]^{3+}$ complexes were synthetized and characterized by XRD. Photophysical studies highlight important effects of symmetry on emission band structurations and width as well as on $Cr(^2E)$ excited state lifetime, which reach the millisecond range below 100 K and several hundred of microsecond at room temperature.

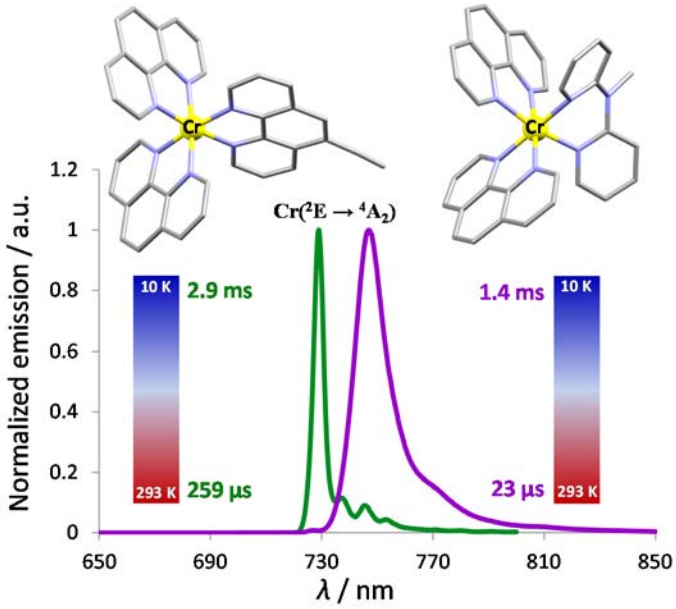

Graphical abstract